DOE/NASA/2593-79/6
NASA TM-79139

GAS-TURBINE CRITICAL RESEARCH AND ADVANCED TECHNOLOGY SUPPORT PROJECT: FY 1978 ANNUAL REPORT

John S Clark, Carl E Lowell, Richard W Niedzwiecki and Joseph J Nainiger
National Aeronautics and Space Administration
Lewis Research Center

June 1979

Prepared for
U.S. DEPARTMENT OF ENERGY
Office of Fossil Energy
Divison of Fossil Fuel Utilization

NOTICE

1 Report No	2 Government Accession No	3 Recipient's Catalog No
NASA TM-79139		

4 Title and Subtitle	5 Report Date
GAS-TURBINE CRITICAL RESEARCH AND ADVANCED TECHNOLOGY SUPPORT PROJECT FY 1978 ANNUAL REPORT	June 1979
	6 Performing Organization Code

7 Author(s)	8 Performing Organization Report No
John S Clark, Carl E Lowell, Richard W Niedzwiecki, and Joseph J Nainiger	E-9986
	10 Work Unit No

9 Performing Organization Name and Address	11 Contract or Grant No
National Aeronautics and Space Administration Lewis Research Center Cleveland, Ohio 44135	
	13 Type of Report and Period Covered
12 Sponsoring Agency Name and Address U S Department of Energy Division of Fossil Fuel Utilization Washington, D C 20545	Technical Memorandum
	14 Sponsoring Agency ~~Code~~ Report No DOE/NASA/2593-79/6

15 Supplementary Notes

Prepared under Interagency Agreement EF-77-A-01-2593

16 Abstract

The report summarizes the technical progress made during the first 15 months of a planned 40-month project to provide a critical-technology data base for utility gas-turbine systems capable of burning coal-derived fuels Tasks were included in the following areas (1) combustion - to study the combustion of coal-derived fuels and the conversion of fuel-bound nitrogen to NO_x, (2) materials - to understand and prevent hot corrosion, and (3) system studies - to integrate and guide the other technologies Significant progress has been made Combustion test rigs are being designed and built to study NO_x generation A statistically designed hot-corrosion test was completed, and a hot-corrosion-life prediction model was developed Barium was identified as a fuel additive that inhibits hot corrosion Several advanced ceramic thermal-barrier coatings demonstrated improved resistance to potential coal-derived fuel contaminants A computational analysis of thermal-barrier coatings on water- and steam-cooled turbines indicated substantial improvement in performance and specific power over those of an uncoated system

17 Key Words (Suggested by Author(s))	18 Distribution Statement
Gas turbine, Coal-derived fuel, Hot corrosion, Combustion, Thermal barrier coatings, Combined cycle, Power generation, Ceramics	Unclassified - unlimited STAR Category 44 DOE Category UC-90f

19 Security Classif (of this report)	20 Security Classif (of this page)	21 No of Pages	22 Price*
Unclassified	Unclassified		

* For sale by the National Technical Information Service Springfield Virginia 22161

DOE/NASA/2593-79/6
NASA TM-79139

GAS-TURBINE CRITICAL RESEARCH AND ADVANCED TECHNOLOGY SUPPORT PROJECT: FY 1978 ANNUAL REPORT

John S. Clark, Carl E. Lowell, Richard W. Niedzwiecki, and Joseph J. Nainiger
National Aeronautics and Space Administration
Lewis Research Center
Cleveland, Ohio 44135

June 1979

Prepared for
U. S. DEPARTMENT OF ENERGY
Office of Fossil Energy
Division of Fossil Fuel Utilization
Washington, D. C. 20545
Under Interagency Agreement EF-77-A-01-2593

SUMMARY

This report summarizes the technical progress made during the first 15 months of a planned 40-month project to provide a critical-technology data base for utility gas-turbine systems capable of burning coal-derived fuels. Coal-derived fuels present two major problems to utility gas turbines. First, they are typically high in organically bound nitrogen, which is converted in the combustion process to oxides of nitrogen (NO_x). Second, they contain trace-metal contaminants that can lead to hot corrosion in the turbine hot sections.

A combustion task is under way to address the first problem. A literature survey of coal-derived-fuel properties was completed and an NO_x emission model was developed. Test rigs have been designed and are being built to experimentally study the conversion of fuel-bound nitrogen to NO_x.

To address the second problem, a statistically designed series of hot-corrosion burner rig tests were conducted to measure the corrosion rates of typical gas-turbine alloys with several fuel contaminants. The resultant data have been correlated into a hot-corrosion-life prediction model. Another approach to solving the hot-corrosion problem is to use a fuel additive that inhibits hot corrosion. Barium has been identified as a particularly beneficial fuel additive. Still another approach to preventing hot corrosion is to protect the hot components with a coating. Ceramic thermal-barrier coatings offer potential corrosion resistance as well as thermal protection. Several advanced thermal-barrier coatings have demonstrated promising hot-corrosion resistance.

Systems studies were also conducted to help integrate and guide the technological efforts. An analytical study of thermal-barrier coatings used in conjunction with water- and steam-cooled turbine airfoils indicated substantial performance improvement over that of an uncoated system. Specific power also increased, which should lead to lower capital costs.

E-9986

INTRODUCTION

The Critical Research and Advanced Technology Support Project (CRT) is directed toward providing a critical-technology data base to support the development of gas-turbine systems capable of burning coal-derived fuels. The CRT project was begun by the NASA Lewis Research Center and the ERDA Office of Fossil Energy on June 30, 1977 Upon creation of the Department of Energy on October 1, 1977, the project was assigned to the DOE Division of Power Systems, which has been renamed the Division of Fossil Fuel Utilization. This report summarizes the technical progress at the end of the first 15 months of the planned 40-month project.

The focus of the effort in this project has been on "critical" technologies - those problems that must be resolved before coal-derived fuels can be considered viable for use in gas turbines. Two technologies (tasks) have been identified. combustion and materials. Emphasis in the combustion task is on reducing both thermal and fuel-bound NO_x emissions. Emphasis in the materials task is on trace-metal contaminants in coal-derived fuels, which can lead to unacceptable hot corrosion in the turbine hot section Several approaches to solving the materials problem are being investigated, including developing a hot-corrosion-life model and using fuel additives or protective coatings. Systems studies were made to help integrate and guide the materials and combustion tasks

The technical objectives of the CRT project are

(1) To develop combuster concepts that will use coal-derived liquid fuels in an environmentally acceptable manner

(2) To develop a hot-corrosion data base for materials exposed to combustion products of coal-derived fuels and to correlate these data in a hot-corrosion-life prediction model

(3) To develop ceramic coatings that have acceptable life in coal-derived-fuel combustion products

(4) To study the trade-offs among various gas-turbine technologies, operating conditions, and component designs

The following sections discuss the purpose of each task, our approach to it, and its present status. A detailed discussion of results is included where appropriate.

TASK 1.0 - SYNCRUDE AND SYNFUEL CHARACTERIZATION AND COMBUSTION STUDIES

Most utility gas turbines currently use relatively high-quality hydrocarbon fuels, such as No. 2 gas-turbine fuel oil or natural gas. A limited number of utility gas turbines are equipped to fire heavier fuels, such as No 6 or residual fuel oils. However, the additional capital cost of fuel cleanup equipment for these turbines is high. Operating and maintenance costs are also higher than with cleaner fuels, and the heat rate is usually higher because turbine firing temperatures are downrated In the future, utility gas turbines will probably use liquid synthetic fuels from coal. These fuels will probably be lower in quality than current petroleum distillate fuels and could require additional refining, which would further increase their already relatively high costs Minimizing the processing required to remove trace impurities and the hydroprocessing required to convert aromatic hydrocarbons to saturated hydrocarbons would reduce these costs.

The objectives of task 1.0 are (1) to establish a data base of the properties of coal-derived fuels (subtask 1.1) and (2) to evolve combustion technology so that these fuels can be used in utility gas turbines with minimum NO_x pollution (subtasks 1.2, 1.3, and 1.4). This task is also planned to provide data to aid in establishing fuel specifications for advanced gas-turbine systems burning coal-derived fuels in an environmentally acceptable manner. Each subtask is described in the following sections.

SUBTASK 1.1 - SYNCRUDE AND SYNFUEL CHARACTERIZATION

The objective of subtask 1.1 is to systematically assemble existing data on the elemental composition, structural characteristics, and physical and chemical properties of liquid and gaseous synthetic fuels derived from coal.

A literature survey was conducted in early FY 1978 to compile existing property data for coal-derived fuels. A bibliography of reports on liquid fuels and low-Btu gases was assembled. This survey included - but was not limited to - the development and upgrading of DOE-sponsored synthetic-fuel pilot plants. A report describing the results of this literature survey will be published in 1979. Very little detailed, comprehensive characterization data exist at this time. An update of this survey is planned in 1979, since current synthetic-fuels programs are very active.

SUBTASK 1.2 - NO_x EMISSION MODELING

The objectives of subtask 1.2 are to analytically determine, through combustion modeling, how combustor operating conditions affect the conversion of fuel-bound nitrogen to NO_x and to determine the minimum theoretical NO_x emission levels obtainable from synthetic fuels containing significant quantities of organic nitrogen compounds. Several approaches have been investigated. An existing well-stirred-reactor model (ref. 1) has been modified to incorporate fuel-bound-nitrogen components. This model, although it forecasted trends, did not provide acceptable results over the entire parameter ranges of interest, especially at equivalence ratios much greater than stoichiometric An alternative model is currently being studied (ref. 2). This model contains detailed chemical kinetics schemes and has been modified by the addition of stirred-reactor equations A parametric survey of the model over an extended range of combustor performance and flow conditions is being conducted. The model will be verified and optimized by using the flame-tube test data described in the following section.

SUBTASK 1.3 - FLAME-TUBE EXPERIMENTS

The objectives of subtask 1.3 are to experimentally investigate the conversion of fuel-bound nitrogen to NO_x, to determine the factors controlling fuel-bound-nitrogen conversion, to determine the minimum achievable levels of that conversion, and to provide experimental verification of the NO_x model. A two-stage combustion flame-tube rig incorporating independent airflow control to each combustion zone will be used for these tests. A propane-toluene-pyridine fuel system has been designed to obtain baseline data and to vary the hydrogen-carbon ratio and the fuel-bound-nitrogen level, respectively.

First, testing will be conducted with propane for a "clean"-fuel data base. Next, toluene and pyridine will be blended and tested. Later, verification testing will include representative liquid fuels. Testing will be conducted at inlet-air temperatures to 538° C (1000° F), inlet pressures to 6 atmospheres, a range of primary-zone equivalence ratios from 0.5 to 5.0, and three residence times. Exhaust gas will be sampled for NO, NO_x, CO, HC, CO_2, and smoke concentrations. The NO_x levels will be compared with predicted results from subtask 1.2. Testing is scheduled to be completed in FY 1979

SUBTASK 1 4 - COMBUSTOR SECTOR TESTS

The objectives of subtask 1.4 are to evolve and evaluate experimental combustors capable of burning coal-derived fuels in an environmentally acceptable manner. Testing will be conducted at representative utility gas-turbine temperatures and pressures, in single 20-centimeter (8-in) tubular combustors Three levels of combustor technology will be evaluated - minor modifications, major modifications, and very major modifications "Minor modifications" are modifications to existing combustor concepts that can be used to retrofit existing engine combustors These modifications should improve fuel flexibility and durability but have limited potential to reduce NO_x. "Major modifications" involve new, advanced-technology designs and would replace existing combustors. These designs will be constrained to fit within an existing representative combustor envelope. They provide greater performance improvement and larger emission reductions than the minor modifications. "Very major modifications" involve the most advanced combustor designs and will incorporate emission reduction and performance features not currently within the state of the art, such as variable geometry. Advanced multi-burning-zone designs will be incorporated in the major and very major modifications

Testing will be conducted at simulated utility gas-turbine conditions. Operating conditions from engine cranking to full power will be investigated. Heavy oil fuels, doped heavy oil fuels, and coal-derived fuels (as available)

will be tested. Combustion efficiency, liner temperatures, exit temperature distributions, gaseous emissions, smoke levels, and deposition characteristics will be investigated. Tests will be run with thermal-barrier coatings on the inside of the combustor liner to determine their effects on performance and durability Testing is scheduled for FY 1979 and FY 1980.

TASK 2.0 - LONG-LIFE-MATERIALS

CORROSION EVALUATION

Coal-derived fuels contain varying amounts of trace metals, and certain of these fuel contaminants can lead to hot corrosion in the gas-turbine hot section. Task 2 0 was undertaken to contribute to the understanding and prevention of hot corrosion.

SUBTASK 2.1 - ADVANCED-TURBINE-MATERIALS

TEST AND EVALUATION

Subtask 2 1 was planned to study advanced utility turbine materials (such as high-strength alloys and ceramic thermal-barrier coatings) in the combustion products of coal-derived fuels - both actual and simulated.

Subtask 2.1.1 - Initial Screening Tests

The initial screening tests were run with simulated coal-derived fuels. In these tests, selected contaminants were added to a clean fuel (1) to isolate the corrosion effects of a given contaminant and concentration and (2) to determine the interrelationships of fuel impurities, deposits, and high-temperature corrosion.

Subtask 2.1.1.1 - Doped-fuel-tests. - The doped-fuel tests were run to determine the corrosion effects of many different fuel impurities on several turbine alloys so that the combustion-product corrosivity of a coal-derived turbine fuel could be estimated from its impurity content. In FY 1978, accelerated atmospheric burner rig tests were completed on four cast airfoil alloys (IN-100, IN-792, Mar M-509, and U-700) for 100 1-hour cycles in a Mach 0 3 gas. A burner rig test is shown in figure 1, and the alloy compositions are shown in table I. The test material temperatures ranged from 800° to 1100° C (1472° to 2012° F), although most of the runs were made at either 900° or 1000° C

(1652° or 1832° F). The impurities studied - sodium, potassium, magnesium, calcium, and chlorine - were injected parametrically (individually and in combination) as water-soluble chlorides and sulfates into the burner rig combustor. The range of concentration was from 0.04 to 4.95 ppm of the combustion gases (0.8 to 100 ppm fuel equivalent) to achieve the accelerated corrosion Most of the tests were run at 0.2 or 1.0 ppm in the gas (about 4 to 20 ppm fuel equivalent) The sulfur content of the fuel was 0.05 percent. Jet A aircraft turbine fuel was the primary heat source for this test. The element combinations, the number of runs, and the test order were established statistically to obtain the most corrosion information with the fewest runs (table II). The corrosion data were evaluated in blocks of 16 runs so that the statistical test design could be revised as necessary. For example, the eight variables of the initial set required about 80 burner rig runs Final evaluation of the data (primarily metal recession) was made by linear regression analysis for each alloy, which gave the corrosivity of the dopants as a function of composition and concentration.

Briefly, the doped-fuel test plan, outlined in table II, was as follows: The test variables included the impurities sodium, potassium, magnesium, calcium, and chlorine added as water-soluble chlorides and sulfates, temperature; and alloy composition The values studied in the tests are given in a footnote to the table. Coding for the test matrix is shown graphically for two variables in figure 2·

Star points A^+, B^+, A^-, B^-

A^+ Variable A at maximum value, variable B at center-point value (CP)

A^- Variable A at minimum value, variable B at CP value

Center points· Both variables at CP values

Corner points AB, A, B, (-)

AB: Both variables included at next-to-highest concentrations

(-): Both variables included at next-to-lowest concentrations

B· Variable B at next-to-highest concentration; variable A at next-to-lowest concentration

The seven-dimensional test matrix shown in table II is similarly coded. The center points are included to analyze variations from rig to rig and possible variations with time.

The original test plan used the following variables the compounds NaCl, Na_2SO_4, KCl, K_2SO_4, M_gCl_2, and $CaCl_2$; temperature; and time. The resultant data indicated that an equally good fit could be made when concentrations of the elements Na, K, Mg, Ca, and Cl were used as variables However, since chlorine was present in four of the six compounds used (four of the impurities

were added as chlorides), the matrix, when considered from the standpoint of concentrations of elements, was seriously unbalanced to high values of chlorine. Thus eight additional runs were designed to rebalance the matrix, and two runs were designed to further confirm the interchangeability of the elements and compounds. This latter goal was achieved by adding the metals as nitrides instead of chlorides as found in the center-point runs of the original matrix. While final analysis of all the data is incomplete, sufficient work has been done to show that the center-point data are the same for either additive mode. Although the effects of the impurities Na, K, Ca, Mg, and Cl and temperature have not been completely evaluated, some conclusions can be drawn:

(1) The forms in which the corrosion elements studied are introduced are not important to the corrosion process.

(2) Many interaction effects among the elements both increase corrosion and decrease it As a result, simple tests of single-element additions cannot predict how they will act in combination.

(3) Because each alloy reacts differently to the impurity combinations, it is difficult to make generalizations about the response of alloy classes (e g , Ni-base or Co-base alloys) to hot corrosion

All tests planned for FY 1978 were completed. Final analysis of all the data is currently in progress, and a report is planned for early 1979.

Subtask 2.1.1.2 - Additive tests. - The objective of the additive tests was to evaluate the effectiveness of several potential fuel additives in reducing impurity-induced corrosion. The testing and evaluation methods were the same as those for the doped-fuel tests The same alloys were evaluated The corrosive element (sodium sulfate) was introduced into the combustion products of the sulfur-containing fuel as NaCl The potential inhibitors (Mg, Si, Al, Cr, Ce, Zn, Ca, and Ba) were also introduced as a water solution except for silicon, which was used as a collodial suspension The success of the additives was judged by minimized weight change and metal thickness loss, as well as by weight gain resulting from heavy, inert deposits Table III gives the forms and concentrations of the additives used in these tests

The planned additive tests were successfully completed in FY 1978 and a report was issued (ref 3) The results of these tests were as follows

Aluminum and silicon The aluminum additive had little, if any, effect on the hot-corrosion attack of sodium on the nickel-base alloys tested, U-700 was not tested in this series (fig. 3). On the other hand, the corrosion of Mar M-509 and 304 stainless steel was substantially reduced, although considerable hot corrosion of Mar M-509 still took place in spite of the aluminum. Silicon, which had been tested as a corrosion inhibitor in earlier work (ref 4), markedly reduced hot corrosion in all but the most corrosion-prone alloy, IN-100 However increasing the silicon addition from 0.5 to 1.8 ppm had little effect except

on the 304 stainless steel Neither silicon nor aluminum can be said to "stop" hot corrosion in cobalt- or nickel-base alloys

Evaluation of the 304-stainless-steel results is hampered by the fact that, in oxidation only, the chromia-forming steel loses excessive weight because its protective oxide is volatilized. Any deposit, either a normally aggressive Na_2SO_4 or an inert oxide, reduces this volatilization and, as a result, reduces the metal consumption rate of 304 stainless steel. Therefore, the additives' effectiveness in reducing sodium attack can be compared among themselves but cannot be compared directly to the results for 304 stainless steel.

Chromium, iron, and zinc The chromium additive was included in these tests to compare this type of additive technique with organometallic additions directly to the fuel (refs 5 to 6) In the present study, adding chromium roughly halved (fig. 4) the hot corrosion, except for 304 stainless steel, in which no effect was noted, this result is quite similar to those of reference 6. In contrast, iron had little or no effect except on the 304, in which hot corrosion was substantially reduced Surprisingly, zinc was even more effective than chromium in reducing hot corrosion of all the alloys, although the results were erratic and in no case was the metal recession reduced to near oxidation levels

Magnesium, calcium, and barium: The alkaline earths were the most interesting group of additives in that all three elements greatly reduced the effects of hot corrosion for all alloys tested (IN-738 was not tested with Ba), as shown in figure 5 Of all the elements tested, barium stands out as having the most consistently large effect, in most cases the attack was reduced to negligible differences from the minor attack observed in oxidation tests All the alloys in the barium inhibitor test had metal recessions of less than 50 micrometers, that is especially dramatic for IN-100, which lost over 2000 micrometers in the presence of the sodium-doped gases alone but less than 50 micrometers when barium was added Although the effect of magnesium additions was comparable for IN-792, IN-738, and U-700, they were much inferior to barium in reducing the attack on IN-100 and Mar M-509 The thickness change data are supported by the outward appearances and the microstructures of the alloys An example of the effect of alkaline earth additives is shown in figure 6 for IN-792 The extreme conditions are the NaCl additive only on the left and the oxidation on the right As anticipated from the thickness change values, the samples tested with magnesium and barium inhibitors showed only slight attack. The specimens with the calcium inhibitor showed less attack than in the presence of NaCl alone, but more than with the barium or magnesium inhibitors. Also evident are the nonsoluble deposits on the calcium-inhibited sample Such deposits were also observed, but to a lesser extent, on the barium-inhibited sample and were observed least on the magnesium-inhibited sample Thus, even though the hot-corrosion attack was greatly reduced, the effect of these

deposits on fouling and their ease of removal would have to be evaluated before their potential for commercial use could be fully assessed

These effects are shown more clearly at higher magnification on specimen cross sections. Figures 7(a) and 8(a) show the typical hot-corrosion microstructures for a nickel- and a cobalt-base alloy, respectively. The nickel alloy was characterized by an extensive depletion zone, nickel sulfides, and a heavy oxide scale of predominantly NiO. The cobalt alloy was characterized by carbide depletion and extensive grain-boundary attack. Figures 7(e) and 8(e) show typical burner rig oxidation microstructures (note decrease in magnification), which are characterized by slight depletion zones and thin oxide scales. Magnesium and barium additions yielded microstructures that were more characteristic of oxidation than of hot-salt corrosion. The calcium-inhibited samples showed more attack but were still closer in appearance to oxidation specimens than to uninhibited hot-corrosion specimens

As pointed out earlier, inert deposits were formed on the alloys when barium or calcium salts were used to inhibit corrosive attack. In all cases the deposit from the magnesium additions was MgO; however, the barium and calcium deposits were sulfates. In attempting to assess the potential deleterious fouling effect of such deposits, it should be remembered that the levels of both the corrodent and the inhibitor were a factor of about 50 higher than would be expected in an actual engine. Therefore, to a first approximation the deposit was forming at a rate 50 times faster Thus, although there might be a problem with deposition when using barium additives, it is far from certain. This potential fouling problem will be evaluated in follow-on efforts. Another factor would be cost. Although a detailed cost analysis must be made, it is very unlikely that cost will be a significant factor. Additive cost would have to be balanced against downtime and materials costs, but such a cost analysis is outside the scope of this report.

Subtask 2 1.1.3 - Thermal-barrier coatings. - This subtask is divided into two major activities: The first is aimed at improving the resistance of thermal-barrier coatings to the harsh environment expected in the combustion products of coal-derived fuels The second is aimed at improving the bond-coating layer to provide better thermal-barrier adherence and both hot-corrosion and oxidation resistance.

Subtask 2.1.1 3.1 - Dirty-fuels tests· Mach 0 3 burner rig tests were run to evaluate many advanced thermal-barrier coatings in simulated coal-derived-fuel combustion products. Cast-superalloy, hollow erosion bars, shown in figure 9, were plasma sprayed with a NiCrAlY bond coating and the advanced ceramic coatings. The specimens were then mounted - eight at a time - in a multiple-specimen test fixture (fig 10). The fixture was then mounted in the

Mach 0 3 burner rig (fig. 11) and cyclic tests were run The hot gas stream was maintained at 1370° C (2500° F; the calculated adiabatic flame temperature) for an hour and then cooled rapidly to room temperature with an ambient air jet The ceramic outer surface temperature was measured with an optical pyrometer and was maintained at 982° C (1800° F) The metal substrate temperature was measured with thermocouples and was maintained at 843° C (1550° F). The results of these tests are presented in reference 7 and are summarized here.

A wide range of conceptual thermal-barrier coating systems were evaluated. Nominal chemical compositions of the bond and thermal-barrier coatings are presented in table IV Coating 1 is referred to as the "standard" thermal-barrier coating (STBC): It was developed for clean-fuel aircraft applications and is a fully stabilized zirconium oxide. However, this coating was shown to have a short life in combustion products of fuels with sodium and vanadium contamination (ref 8) To effect the desired improvement in corrosion resistance, several NASA Lewis Research Center investigators suggested coating variations that involved the following approaches. (1) modifying the composition of the oxides and bond coatings, (2) sealing the oxide with a more dense oxide overcoating, (3) heating the hollow erosion bar before plasma spraying the oxide in order to stress relieve it, (4) impregnating and sealing the oxide with silica, and (5) heat treating the thermal-barrier system on hollow erosion bars to selectively establish a crack network to prevent massive spalling.

Figure 12 is a compilation of the results of Mach 0 3 burner rig tests of all the coatings for times to 1000 hours Thermal-barrier-coated specimens were removed from testing, and the number of 1-hour cycles was recorded after the coating had spalled over approximately one-fourth of the leading-edge hot zone

Several modified ZrO_2-Y_2O_3/NiCrAlY thermal-barrier systems were more spall resistant than the standard thermal-barrier coating system ZrO_2-12Y_2O_3/Ni-16.2Cr-5 6Al-0 6Y (STBC), which spalled before 80 hours of exposure. These modified systems included the ZrO_2-8Y_2O_3/N-16 4Cr-5 1Al-0 15Y (coating 9) which was optimized in burner rig tests, natural-gas-fired torch tests, and furnace tests (ref. 9) and failed after 384 1-hour exposure cycles. Also, the ZrO_2-12Y_2O_3/Ni-31Cr-12Al-0.6Y coating (coating 11) failed after 178 1-hour cycles. The Y_2O_3-ZrO_2-12Y_2O_3/Ni-16.2Cr-5.6Al-0 6Y coating (coating 6) was removed from testing after 320 cycles because of continuous hot-section surface microspalling that began after 40 cycles. Coating loss, however, was extensive in cooler regions outside the hot zone. For all these systems, spalling occurred near the oxide - bond-coating interface with approximately 0 005 to 0 015 centimeter (0.002 to 0 006 in) of oxide remaining on the bond coating. No apparent corrosion of the bond coatings was detected from metallographic analysis of spalled areas.

A number of additional coating systems based on the ZrO_2-Y_2O_3/NiCrAlY system were tested (table IV); their spalling behavior was, for all practical purposes, the same as that of the STBC (coating 1). From the results shown in figure 12, it appears that heat treating the STBC and the Al_2O_3 overcoating had no beneficial effect on spall resistance (coatings 3, 4, and 5). Also, from the limited data, stress relieving the oxide by heating the substrate during oxide application (coating 2) had no effect on spall rate in the Na-V doped combustion gases. Similarly, the spalling rates of the STBC and ZrO_2-18Y_2O_3 coating systems (coating 8) did not differ significantly. However, the data suggest that the optimum level of Y_2O_3 in ZrO_2 thermal-barrier coatings is less than 12 weight percent (coatings 9 and 10). The existence of an optimum level of Y_2O_3 in ZrO_2 was not clearly established in this hot-corrosion burner rig program because different bond coatings were used with the ZrO_2-12Y_2O_3, ZrO_2-8Y_2O, and ZrO_2-4Y_2O_3 thermal-barrier coatings. The importance of the bond coating is shown clearly in the results for coatings 11 and 12. Both the Ni-31Cr-12Al-0.6Y bond coating (coating 11) and the Ni-20Co-18Cr-12.5Al-0.6Y bond coating (coating 12) appear to result in better thermal-barrier coating life than the STBC bond coating (Ni-16.2Cr-5.6Al-0.6).

Several new duplex coating systems were tried in the program in addition to the ZrO_2-based thermal-barrier coatings (table IV and fig. 12) Of the duplex coatings tested, one based on Ca_2SiO_4 (coating 13) reached 675 1-hour cycles before spalling. Also, a cermet coating (ref. 10) of 50-volume-percent MgO and 50-volume-percent Ni-19.6Cr-17.1Al-0.97Y (coating 16) survived 1000 1-hour cycles without spalling. These two coatings had significantly better hot-corrosion resistance than the four STBC specimens, which all spalled before 80 cycles A metal substrate temperature of 843° C (1550° F) was measured during the temperature calibration run for both Ca_2SiO_4- and ZrO_2-12Y_2O_3-coated bars. Therefore, the Ca_2SiO_4 and ZrO_2-12Y_2O_3 coatings are approximately equivalent in thermal insulating ability. The thermal conductivity of the cermet coating (coating 16) is much higher than the conductivities of the other coatings. However, it was run at the same hot-gas temperature as the other coatings, T_{gas} = 1370° C (2500° F), and at the same coolant conditions. Accordingly the cermet surface temperature was less than 982° C (1800° F), and the substrate metal temperature was somewhat greater than 843° C (1550° F) - approximately the same average temperature as for the other coatings tested.

The degradation modes of the Ca_2SiO_4- and MgO-NiCrAlY-coated specimens are distinctly different Erosion, corrosion, and possible microspalling appear to be responsible for a 50 percent reduction in MgO-NiCrAlY coating thickness. No macrospalling was observed for this coating system

The Ca_2SiO_4 coating cracked and subsequently macrospalled near the bond-coating - Ca_2SiO_4 interface, similar to the spalling of the ZrO_2-based thermal-barrier coating. Like the other specimens tested, no apparent corrosion of the bond coatings was detected Coatings 14 and 5, the CeO_2 and $ZrSiO_4$ coating systems, respectively, spalled sooner than the STBC

Single-specimen burner rig tests were also run to determine the sensitivity of the standard thermal-barrier coating (STBC) to sodium and vanadium The results of these tests are also presented in reference 7 and summarized herein (fig. 13). Coated specimens were removed from testing when the coating had spalled over approximately one-fourth of the leading-edge hot zone At an equivalent fuel impurity concentration of 5 ppm sodium plus 2 ppm vanadium, the thermal-barrier coating spalled after forty-three 1-hour cycles When thermal-barrier-coated specimens were tested with fuel impurity levels of 5 ppm sodium only or 2 ppm vanadium only, the coated specimens spalled at ninety-two and twenty-five 1-hour cycles, respectively. Thus from this limited study, vanadium appears to be more detrimental to these coatings than sodium. At 0.2 ppm vanadium, the coated specimen spalled after 200 1-hour cycles. However, when the sodium level was reduced in an equivalent manner, that is 0.5 ppm sodium, there was no apparent distress of the coating after 1300 1-hour cycles. At this sodium level, useful thermal-barrier coating system life appears to be more a function of the ceramic-thermal-barrier erosion than of slow oxidation or corrosion of the bond coating. As before, there was no apparent reaction of fuel impurities with the bond coating.

In support of these burner rig tests, a basic study was conducted to determine how partially stabilized zirconia powders containing 8-weight-percent yttria would react with powders of the potential combustion product compounds of major fuel-air impurities and with bond coating elements. The powder reactions were monitored as a function of time by using metallographic and X-ray diffraction techniques. These reactions were studied at 1200°, 1300°, and 1400° C (2192°, 2372°, and 2552° F) for 800, 400, and 200 hours, respectively. The results of these tests are presented in reference 11 and are summarized in table V. The zirconia used in these tests contained both cubic and monoclinic phases, with the cubic phase predominate. Table V lists all the chemical compounds used in this investigation and the products of their reactions with zirconia at 1200°, 1300°, and 1400° C (2192°, 2372°, and 2552° F). It also includes a column marked with letters N or Y indicating that no reaction took place or that there was a partial or complete reaction.

Based on the results, the chemical compounds that were used to react with zirconia can be divided into four distinct groups:

Group 1. Chemical compounds that did not react with zirconia: Na_2SO_4, K_2SO_4, Cr_2O_3, Al_2O_3, and NiO

Group 2. Chemical compounds that reacted completely with zirconia: $CaCO_3$, (CaO), $BaCO_3$ (BaO), and $BaSO_4$

Group 3. Chemical compounds that reacted preferentially with monoclinic ZrO_2: Na_2CO_3 (Na_2O), K_2CO_3 (K_2O), $CoCO_3$ (CoO), Fe_2O_3, MgO, SiO_2, and ZnO

Group 4. Chemical compounds that reacted preferentially with cubic ZrO_2: V_2O_5 and P_2O_5 in form $(NH_4)_2HPO_4$.

In actual practice, thermal-barrier coatings will be used in very complex, hostile environments. The information obtained from this investigation should be useful, however, in analyzing coating failure mechanisms and in developing more fuel-tolerant thermal-barrier coatings. It seems significant, since sodium, potassium, and sulfur will probably always be present in gas-turbine fuels, that neither Na_2SO_4 nor K_2SO_4 - both of which are corrosive to metallic surfaces - reacted with monoclinic and cubic zirconia. The following observations can also be drawn from the results:

(1) The high-temperature reactivity of CoO and Fe_2O_3 and monoclinic zirconia seems to rule out CoCrAlY and FeCrAlY alloys as the bond-coating material if the bond-coating temperature is to be very high

(2) Zirconia thermal-barrier coatings might have reduced life, because of cubic-phase stabilization, in environments containing iron oxide particles (near steel mills or foundaries, or in the combustion products of a coal-derived fuel that contains relatively large quantities of iron as a trace element).

(3) Barium (a potential hot-corrosion-inhibiting gas-turbine fuel additive) would probably be particularly harmful to zirconia thermal-barrier coatings. (It would convert the coating to $BaZrO_3$.)

Subtask 2.1.1 3.2 - Bond-coating optimization: The objective of these tests is to improve the corrosion resistance of the bond coating and the adherence of the thermal-barrier coating. Cyclic furnace tests were run to determine the durability of bond coatings alone and that of bond coatings used with thermal-barrier coatings deposited on nickel- and cobalt-base superalloys (B-1900 + hafnium and Mar M-509, respectively) A total of 151 specimens were tested in FY 1978; some post-test metallographic analyses remain to be completed. Cyclic furnace oxidation testing to 750 hours at 982° C (1800° F) was completed with the standard thermal-barrier coating (STBC), ZrO_2-$12Y_2O_3$, deposited on four plasma-spray-deposited and two sputter-deposited bond coatings. The results of these tests are summarized as follows:

(1) The sputter-deposited bond coatings were very much smoother than the plasma-spray-deposited bond coatings and did not adhere as well to the thermal-barrier outer layer.

(2) The number of cycles to first external crack varied greatly in these tests.

(3) Metallographic analysis of all specimens that survived to 750 cycles with no visible external cracks showed internal crack initiation

Subtask 2.1 2 - Actual-Fuel Tests

The actual-fuel tests were planned to experimentally determine the corrosivity of the combustion products from an actual coal-derived fuel and to compare this corrosivity with the results of the life prediction model (subtask 2.2). Forty-five hundred gallons of SRC-II naphtha was sent by DOE from the Fort Lewis, Washington, pilot plant to the NASA Plum Brook Station in Sandusky, Ohio. The fuel was transferred from the rail car to a specially refurbished NASA fuel trailer. The fuel trailer was equipped with new valves and seals and a recirculation system to ensure a uniform fuel mixture during the long-term testing. During checkout of the recirculation system, an emergency shutoff valve became plugged or stuck and about 1700 gallons of the fuel spilled. There should be sufficient fuel remaining to complete the 1000-hour burner rig test, but the spill delayed startup of the test.

SUBTASK 2.2 - LIFETIME PREDICTION ANALYSIS

In the lifetime prediction analysis the data generated in the doped-fuel tests (subtask 2.1.1.1) were assembled and correlated into mathematical models that can be used to predict metal recession rates as a function of fuel contaminant levels for the four turbine alloys studied - IN-100, U-700, IN-792, and Mar M-509. The metal recession data were analyzed by regression analysis as a function of exposure time and were compared according to goodness of fit, reproducibility, and predictability. All the measurements made in FY 1978 have been incorporated into the regression analysis.

The data for each alloy were correlated with an equation of the form

$$\log(\Delta th_i) = a_i + b_i \log(\text{Time}) \pm \sigma$$

where

Δth_i thickness change for alloy i
a_i constant for alloy i
b_i constant for alloy i
σ deviation

Other "second-order" variables, such as rig-to-rig variations, fuel-air ratio effects, and flow-rate variations, were studied and were found to be small. Table VI summarizes preliminary correlations for 50 data points. Also shown

are the standard error of estimate and the predicted thickness change after 200 hours. A graphic example of the data correlation is shown in figure 14 for IN-100. Also shown in the figure are the four experimental 200-hour thickness change values and the range of one standard deviation (dashed lines in fig.). The 200-hour data for all the alloys fall within the one-standard-deviation band as well.

SUBTASK 2.3 - AIRFOIL COOLING-HOLE PLUGGING

This subtask was undertaken to estimate the potential of cooling-hole plugging in the combustion environment of coal-derived fuels. Two airfoil cooling schemes were planned to be studied is FY 1978:

(1) Film cooling - with relatively large coolant holes and high coolant velocity

(2) Transpiration cooling - with many small holes and low coolant velocity

Short burner rig tests, similar to the tests reported in reference 12, were planned. Tests of film-cooled blades were completed and a report was published (ref. 13). However, no transpiration-cooled airfoils were available, and these tests have been postponed. The film-cooled-blade test results (ref. 13) are summarized here.

Two types of fuel contaminant levels were chosen for the film-cooled-blade tests. These compositions are shown in table VII in parts per million in the combustion gas (20 to 30 times the levels expected in a typical coal-derived fuel). Dopant A proportions correspond to a typical coal-derived fuel such as SCR-II; dopant magnitudes were chosen to accelerate testing. Dopant B is exactly the same as dopant A, except for the 0.5-ppm phosphorus Phosphorus was noted in reference 12 to be extremely critical in terms of deposit "stickiness"; small quantities of phosphorus can lead to rapid deposit buildup and hole plugging. Phosphorus has not been detected in fuel trace-metal analyses to date. However, in reference 8, phosphorus deposits were detected, even though it was not thought to exist in the fuel. A possible explanation for this apparent contradiction is that, when the fuel is analyzed for trace metals, the phosphorus is lost - through volatilization, for example.

Figure 15 is a schematic diagram of the test rig. Doped hot gas from the burner rig was directed onto the leading edge of a film-cooled turbine blade. Film-cooling holes on the blade were distributed around the leading edge in a typical "showerhead" configuration. Cooling air for the blade was ducted into the blade and then forced out through the film-cooling holes. The flame temperature was varied as shown in table VIII, and the leading-edge temperature was adjusted at the start of each test to 815° C (1500° F) by adjusting the coolant flow rate. The coolant pressure was then fixed; and, as the cooling holes became plugged, the coolant flow decreased and the leading-edge temperature

increased. The change in leading-edge temperature was monitored

The results of these experiments are tabulated in table IX and are plotted in figure 16. The results of these tests are summarized as follows·

(1) The tests that were run with $(\rho V)_c/(\rho V)_h \leq 1\ 0$

where

ρ density of coolant air or hot gas
V velocity of coolant air or hot gas
c coolant
h hot gas

showed severe hole plugging.

(2) Dopant B (with 0.5 ppm P) was worse than dopant A

(3) For very high coolant flow ratios (>1.0), hole-plugging can be nearly eliminated, depending on the fuel composition These coolant flow quantities and pressure requirements may not be practical, however

The effect of pressure was also studied in reference 13. With a deposition kinetics theory developed by Rosner, et al. (ref. 14), the deposition rate was calculated as a function of pressure. Figure 17 shows the predicted deposition rate of sodium sulfate, which is typical of other deposits formed, as a function of pressure. These calculations indicate that deposition rate increases with pressure; thus, deposition and hole-plugging problems at elevated pressures should be more severe than those observed in the atmospheric burner rig tests. Also, for a 16:1-pressure-ratio turbine, the calculated deposition rates are about 10 times those at 1 atmosphere. Thus, rig dopant levels of 20 to 30 times actual levels should produce deposits in amounts approximately those in utility turbines.

SUBTASK 2.4 - COMBUSTION PRODUCTS ANALYSIS

The objective of the combustion products analysis is to evaluate the capability of an existing, complex, NASA chemical equilibrium computer program to calculate the composition and condensed-phase combustion products. It would use the trace-metal content of the fuel to predict probable deposit compositions and onset temperatures (dewpoints). Input data requirements for the computer program include fuel composition, including trace metals, and thermodynamic data for all the potential chemical compounds and species

The thermodynamic data have been assembled for the complex compositions expected in coal-derived-fuel combustion gases. The program was modified to handle 20 chemical elements and 500 potential species simultaneously. Thermodynamic data were added to the program for titanium, lead, vanadium, silicon, barium, and zinc. The program also included thermodynamic data

for carbon, hydrogen, nitrogen, oxygen, sulfur, chlorine, sodium, potassium, iron, calcium, aluminum, and magnesium. Additional new species were added that contained the elements sodium, potassium, calcium, aluminum, and magnesium. Data for various mixed-metal oxides - such as $NaAlO_2$, Al_2MgO_4, NaV_2O_4, $Na_2Fe_2O_4$, and Mg_2SiO_4 - were also added. It is expected that this program will be continually updated as new thermodynamic data become available for mixed-metal oxides, slags, and glassy phases.

Samples of three streams from the Solvent Refined Coal (SRC) pilot plant are on hand. We plan to use them to obtain experimental deposition data for comparison with the predicted results. Consistent and reliable trace-metal characterization of the samples will be required, however, before the model and deposition tests can be run and the results compared. Accurate, consistent characterization is not readily available, however, as judged by the results from several analytical laboratories on identical samples. An investigation of analytical procedures will continue in FY 1979.

TASK 3 0 - TECHNOLOGY EVALUATION STUDIES

SUBTASK 3.1 - THERMAL-BARRIER-COATING

LIQUID COOLING STUDY

How thermal-barrier coatings (TBC) affect the performance and cost of electricity (COE) of air-cooled, open-cycle-gas-turbine systems has been investigated (refs. 15 to 17). These studies indicate potential reductions in both fuel usage and COE for utility gas-turbine systems that use thermal-barrier coatings. The objective of this subtask is to quantify the performance effect for more advanced steam- and water-cooled gas-turbine combined-cycle systems that use thermal-barrier coatings. A plasma-sprayed, duplex thermal-barrier coating, consisting of a yttria-stabilized zirconia outer layer and a NiCrAlY bond coating was assumed.

The combined-cycle cases studied are indicated in table X. Air-cooled cases, both with and without TBC, were included as a reference or baseline. As shown, three cases were considered for each coolant. In the first two cases (footnote a in table X), the metal-substrate temperature and turbine-inlet temperature were assumed to be the same as for the case without TBC, and the turbine coolant flow rate was reduced. Coating thicknesses of 0.038 and 0.076 centimeter (0 015 and 0.030 in.) were assumed. In the third case (footnote b in table X), the metal temperature and the coolant flow rate were kept the same as for the case without TBC, and the turbine-inlet temperature was increased. A coating thickness of 0.38 centimeter (0.015 in.) was used in this case. The

bond-coating thickness was assumed to be 0.10 centimeter (0.004 in.) for all cases. For the water-cooled combined-cycle cases studied, turbine rotor-inlet temperatures were used (to be consistent with the DOE High Temperature Turbine Technology (HTTT) program). Turbine vane inlet temperatures for these conditions are 1448° C (2639° F) and 1684° C (3062° F), corresponding to rotor-inlet temperatures of 1425° C (2600° F) and 1650° C (3000° F), respectively.

The results of the study are presented in reference 18 and are summarized herein. Substantial performance improvements are indicated. Figure 18(a) compares the performance results for these systems at a reduced cooling-air flow rate. Using TBC reduces the required coolant flow rate and the heat losses in the turbine and thus improves performance. The combined-cycle efficiency improvements with TBC (relative to the efficiencies without TBC) were greater at the higher temperatures, where steam and water cooling were used. At these temperatures the heat losses from the working fluid to the cooled blades or vanes were higher than at the lower temperatures, where air cooling was used. Therefore, the use of insulating TBC has a greater effect. The specific power improvements, as a percentage of the specific power for the cases without TBC, were greater when air cooling was used.

In figure 18(b), the combined-cycle performance is shown for the TBC cases in which the metal temperature and coolant flow rate were held constant and the turbine-inlet temperature was increased. For air and steam cooling at 1205° C (2200° F), figure 18(b), increasing the turbine-inlet temperature improved efficiency more than was shown in figure 18(a) - for a lower cooling-air flow rate. However, for steam cooling at 1425° C (2600° F) and water cooling at 1450° C (2639° F), increasing the turbine-inlet temperature to 1675° and 1733° C (3050° and 3150° F), respectively, did not improve the efficiency as much as that shown in figure 18(a). For the steam-cooled combined cycle without TBC a high percentage of the steam-turbine throttle flow was used to cool the gas turbine at 1675° C (3050° F). This resulted in lower steam-cycle efficiency and thus lower combined-cycle efficiency than those for the steam-cooled combined cycle at the same temperature but with a 0.038-centimeter-(0.015-in -) thick TBC. Likewise, for the water-cooled combined cycles, reducing the heat loss from the turbine gas path by using TBC and holding the turbine-inlet temperature constant (as shown in fig. 18(a)) resulted in greater efficiency improvements than obtained by increasing the turbine-inlet temperature while maintaining the same heat losses. However, the increase in specific power is much greater when the turbine-inlet temperature is increased, and higher specific power results in a lower capital cost on a dollar-per-kilowatt basis and thus a lower cost of electricity.

As shown in figure 18, the steam-cooled combined cycles have lower efficiency and higher specific power than the air-cooled cycles at the same turbine-inlet temperature. Aslo, the water-cooled combined cycles have lower efficiency and higher specific power than the steam-cooled cycles. Care should be taken in comparing the performance of these air-, steam-, and water-cooled combined cycles, since the purpose of this subtask is to compare the performance improvements when using TBC with these three cooling methods, and not to compare the relative benefits of the cooling methods themselves. None of the systems were optimized with respect to performance. For example, selecting other compressor pressure ratios, other steam bottoming cycles, or other configurations than those considered in this analysis would affect the relative performances of combined cycles using these cooling methods. These parameters were selected for this study primarily from the results of previous studies (refs. 19 to 22). Although steam cooling appears to be competitive with water cooling, further detailed parametric performance analyses, beyond the scope of this subtask, would have to be done to verify this conclusion. Also, detailed cost data would be needed to compare the relative economics of steam and water cooling.

SUMMARY OF RESULTS

This report summarizes the technical progress made during the first 15 months of a planned 40-month effort to use coal-derived fuels in utility gas turbines. The project includes critical-research and advanced-technology efforts in combustion, materials, and systems studies. Significant progress has been made toward achieving the technical objectives of this work; this progress is summarized as follows:

1. A literature survey of coal-derived-fuel properties was completed. Very little comprehensive characterization data exist at this time.

2. An analytical oxides-of-nitrogen (NO_x) emission model was assembled

3. A flame-tube combustion rig was designed and built to experimentally study the formation of NO_x in a two-stage configuration

4. A statistically designed doped-fuel test was conducted to study the corrosion effects of various coal-derived-fuel contaminants on four cast airfoil alloys. The data from these tests were correlated in a hot-corrosion-life prediction model.

5. Several fuel additives with the potential to reduce hot corrosion were investigated. Barium provided substantial corrosion protection.

6. Thermal-barrier coatings can also protect turbine hot components from corrosion

7. Several coatings provided substantially longer turbine-component life than a fully stabilized zirconia coating that was developed for use with clean fuels.

8. A basic study was conducted of partially stabilized zirconia reacting with potential coal-derived-fuel contaminants and bond-coating constituents.

9. A study was conducted to estimate the potential cooling-hole plugging in the combustion environment of coal-derived fuels. It was concluded that plugging is a strong function of contaminant levels, plugging can be expected at low coolant flow rates, and plugging can be nearly eliminated at very high coolant flow rates.

10 An existing NASA chemical equilibrium computer program was upgraded to predict probable deposit composition and onset temperatures (dewpoints).

11. An analytical study of thermal-barrier coatings with steam- and water-cooled turbine hardware indicated substantial performance and specific power improvement over that with uncoated airfoils.

REFERENCES

1. Boccio, J. L.; Weilerstein, G ; and Edelman, R. B.: A Mathematical Model for Jet Engine Combustor Pollutant Emissions. (GASL-TR-781, General Applied Science Labs., Inc.; NASA Contract NAS W-2235.) NASA CR-121208, 1973.

2. Bittker, David A.; and Scullin, Vincent J.: General Chemical Kinetics Computer Program for Static and Flow Reactions, with Application to Combustors and Shock-Tube Kinetics. NASA TN D-6586, 1972.

3. Deadmore, Daniel L ; and Lowell, Carl E.: Inhibition of Hot Salt Corrosion by Metallic Additives. DOE/NASA/2593-78/2, NASA TM-78966, 1978.

4. Lee, S. Y , Young, W E , and Vermes, G. Evaluation of Additives for Prevention of High Temperature Corrosion of Superalloys in Gas Turbines. ASME Paper 73-GT-1, Apr. 1973.

5. Decrescente, M. A ; Bornstein, N. S.; and Blizzard, C A. M : Fuel Additives to Inhibit Sulfidation. SAE Paper 760919, Nov. 1976.

6. Lowell, C E.; and Deadmore, D. L.: Effect of a Chromium-Containing Fuel Additive on Hot Corrosion. NASA TM X-73465, 1976.

7. Hodge, Philip E.; et al: Thermal Barrier Coatings: Burner Rig Hot Corrosion Test Results. DOE/NASA-2593-78/3, NASA TM-79005, 1978

8. Bratton, R. J ; Singhal, S C.; and Hays, W : Ceramic Rotor Blade Development - Part I: Ceramic Thermal Barrier Coatings. Semi-Annual Tech. Rep.-4, Westinghouse R&D Center, May 1977.

9. Stecura, Stephan: Effects of Compositional Changes on the Performance of a Thermal Barrier Coating System. NASA TM-78976, 1978.

10. Zaplatynsky, Isidor: Oxidation Behavior of Nickel-Chromium-Aluminum-Yttrium-Magnesium Oxide and Nickel-Chromium-Aluminum-Yttrium-Zirconate Type Cermets. NASA TM X-3466, 1976.

11. Zaplatynsky, Isidor: Reactions of Yttria-Stabilized Zirconia with Oxides and Sulfates of Various Elements. DOE/NASA/2593-78-1, NASA TM-78942, 1978.

12. Deadmore, Daniel L., and Lowell, Carl E.. Plugging of Cooling Holes in Film-cooled Turbine Vanes. NASA TM X-73661, 1977

13. Deadmore, Daniel L.; and Lowell, Carl E Airfoil Cooling Hole Plugging by Combustion Gas Impurities of the Type Found in Coal-Derived Fuels, DOE/NASA/2593-79/1, NASA TM-79076, 1979.

14. Rosner, Daniel E.; et al.. Chemically Frozen Multicomponent Boundary Layer Theory of Salt and/or Ash Deposition Rates from Combustion Gases Combustion Science and Technology. 1978.

15. Amos, David J.· Analytical Investigation of Thermal Barrier Coatings on Advanced Power Generation Gas Turbines (EM-1636, Westinghouse Electric Corp.; NASA Contract NAS3-19407). NASA CR-135146, 1977.

16 Carlson, Nils; and Stoner, Barry L.: Study of Thermal Barrier Coatings on High Temperature Industrial Gas Turbine Engines (PSD-R-109, United Technologies Corp.; NASA Contract NAS3-20067.) NASA CR-135147, 1977.

17. Clark, John S.; Nainiger, Joseph J.; and Hyland, Robert E.: Potential Benefits of a Ceramic Thermal Barrier Coating on Large Power Generation Gas Turbines. ERDA/NASA 5022/77/1, NASA TM-73712, 1977.

18. Nainiger, Joseph J.: Effect of Thermal Barrier Coatings on the Performance of Steam- and Water-Cooled Gas Turbine/Steam Turbine Combined Cycle Systems. DOE/NASA-2593-78/4, NASA TM-79057, 1978.

19. Amos, D J.; Lee, R. M.; and Foster-Pegg, R. W.: Energy Conversion Alternatives Study (ECAS), Westinghouse Phase I. Vol. 5: Combined Gas-Steam Turbine Cycles. (REPT-76-9E9-ECAS-RLV.5-Vol-5, Westinghouse Research Labs.; NASA Contract NAS3-19407.) NASA CR-134941, Vol. 5, 1976.

20. Brown, D. H.; and Corman, J. C.: Energy Conversion Alternatives Study (ECAS), General Electric Phase I. Vol. 2: Advanced Energy Conversion Systems, Part 1: Open-Cycle Gas Turbines. (SRD-76-011-Vol-2-Pt-1, General Electric Company; NASA Contract NAS3-19406.) NASA CR-134948, Vol. 2, Pt. 1, 1976.

21. Comparative Evaluation of Phase I Results from the Energy Conversion Alternatives Study (ECAS) NASA TM X-71855, 1976.

22 High Temperature Turbine Technology Program - Reference Turbine Subsystem Designs, Primary and Backup Concepts FE-1806-27, U S. Dept. of Energy, 1977.

TABLE I. - COMPOSITION OF ALLOYS

Element	Mar M-509	IN-792	IN-738	U-700	IN-100	304 SS
			Composition, wt%			
Cr	23	12.7	16	14 2	10	19
Ni	10	Bal.	Bal.	Bal.	Bal	10
Co	Bal	9 0	8.5	15.5	15	-----
Al	----	3.2	3.4	4 2	5 5	-----
Ti	.2	4.2	3.4	3.3	4.7	-----
Mo	----	2 0	1.8	4.4	3.0	-----
W	7	3.9	3.9	-----	------	-----
Ta	3.5	3.9	.9	-----	------	-----
Nb	----	.9	-----	-----	------	-----
V	----	-----	-----	-----	1.0	-----
Mn	----	-----	.2	<.01	------	2.0
Fe	----	-----	.5	.1	------	Bal.
Si	----	-----	.3	<.1	------	1.0
Zr	.5	.1	.1	<.01	.06	-----
B	----	.02	.01	02	.014	-----
C	.6	.2	.17	.06	.18	.08

TABLE II - DOPED-FUEL TEST PLAN

Block	Rig	Test[a]				
		1	2	3	4	5
1	1	BCEFG	ADE	CP 2	FG	ABCDFG
	2	CDEF	ABCD	BDG	CP 3	(-)
	3	ACG	BCE	ACF	ABEG	CP 4
	4	CDEG	CP 1	BDF	ABEF	ADEFG
2	1	BCF	CD	BDE	AB	CP 5
	2	BCG	ABFG	ADE	ABCDEF	CP 6
	3	ABCDEG	CDFG	EG	EF	CP 7
	4	BDEFG	ACE	ADG	ACEFG	CP 8
3	1	ACDE	CP 10	ABD	ABCEG	BCDG
	2	C	CFG	CP 11	ABDFG	BEFG
	3	CP 9	AF	BE	DEG	AG
	4	BCDF	ACDEFG	ABCEF	CP 12	DEF
4	1	BG	D	BCDE	AEFG	CP 13
	2	ABDEF	ABC	ACDG	BF	CP 14
	3	CEF	ABDEG	ACDF	DFG	CP 15
	4	ABCFG	AE	CEG	BCDEFG	CP 16
5	1	CP 17	F^-	CP 18	C^-	
	2	A^+	F^+	D^+	E^+	
	3	B^-	G^-	E^-	B^+	
	4	C^+	G^+	A^-	D^-	

[a]Where the variables tested (impurities and temperature) are denoted as follows

A - NaCl
B - Na_2SO_4
C - KCl
D - K_2SO_4
E - $MgCl_2$
F - $CaCl_2$
G - Temperature

The concentration (in ppm) in the gas and fuel are denoted as follows

	Gas	Fuel(1.25)
A^-	0.04	1.0
-	02	5.0
CP	45	11.3
A	1.00	25.0
A^+	4.95	121.8

And the temperature (in ^{o}C (^{o}F)) is denoted as follows

G^-	800 (1440)
-	900 (1620)
CP	950 (1710)
G	1000 (1832)
G^+	1100 (2012)

TABLE III. - ADDITIVES USED

Metal	Concentration, ppm[a]	Metal source compound
Aluminum	3	$Al(NO_3)_3$
Silicon	.5	Colloidal SiO_2
Silicon	1.8	Colloidal SiO_2
Chromium	3	$(NH_4)_2 CrO_4$
Iron	↓	$Fe(NO_3)_3$
Zinc	↓	$Zn(NO_3)_2$
Magnesium	↓	$Mg(NO_3)_2$
Calcium	↓	$Ca(NO_3)_2$
Barium	↓	$Ba(NO_3)_2$

[a]Parts per million by weight of metal in the combustion products.

TABLE IV - COMPOSITIONS OF THERMAL-BARRIER AND BOND COATINGS

Coating	Thermal-barrier coating[a]	Bond coating, wt%	Reference	Thermal-barrier coating		Bond coating		Treatments and comments
				Thickness				
				cm	in	cm	in	
1	ZrO_2-12Y_2O_3	Ni-16 2Cr-5 6Al-0 6Y	8	0 038	0 015	0 005 to 0 013	0 002 to 0 005	Only cubic ZrO_2 phase present (standard TBC)
2	ZrO_2-12Y_2O_3	↓	--	038	015	↓	↓	ZrO_2 deposited on 538° C (1000° F) preheated substrate
3	ZrO_2-12Y_2O_3	↓	--	038	015	↓	↓	1000° C (1832° F) induction heat of final coated specimen
4	Al_2O_3/ZrO_2-12Y_2O_3	↓	--	008, 038	003, 015	↓	↓	0 008-cm (0 003-in) plasma spray coating of Al_2O_3[b] over standard thermal barrier
5	Al_2O_3/ZrO_2-12Y_2O_3	↓	--	008, 038	003, 015	↓	↓	1000° C (1832° F) induction heat of coated specimen similar to one using coating 4[b]
6	Y_2O_3/ZrO_2-12Y_2O_3	↓	--	008, 038	003, 015	↓	↓	0 008-cm (0 003-in) plasma spray coating of Y_2O_3 over standard thermal-barrier coating[c]
7	ZrO_2-12Y_2O_3-SiO_2	↓	--	038	015	↓	↓	Ludox-impregnated standard thermal-barrier coating, heat treated 1100° C (2012° F) in vacuum for 1 hr[d]
8	ZrO_2-18Y_2O_3	↓		041	016	↓	↓	Higher Y_2O_3 content
9	ZrO_2-8Y_2O_3	Ni-16 4Cr-5 1Al-0 15Y	9	038	015	↓	↓	Cubic and monoclinic phases present
10	ZrO_2-4Y_2O_3	Ni-16 4Cr-5 1Al-0 15Y	9	041	016	↓	↓	Cubic and monoclinic phases present
11	ZrO_2-12Y_2O_3	Ni-31Cr-12Al-0 6Y[e]	8	041	016	↓	↓	Improved bond coating
12	ZrO_2-12Y_2O_3	Ni-21 0Co-18 8Cr-12 8Al-0 6Y[e]	--	038	015	↓	↓	NiCoCrAlY bond coating
13	Ca_2SiO_4	Ni-16 2Cr-5 6Al-0 6Y	--	↓	↓	↓	↓	Calcium silicate[f]
14	CeO_2	↓	--					Cesium oxide[g]
15	$ZrSiO_4$	↓	--					Zirconium silicate[h]
16	50 vol% MgO - 50 vol% Ni-19 6Cr17 1Al-0 97Y	↓	10	↓	↓	↓	↓	Cermet

[a]Weight percent unless stated otherwise

[b]Aluminum oxide, -270 mesh

[c]Yttrium oxide, -150 + 400 mesh

[d]Colloidal silica

[e]Vendor-certified analyses

[f]Chemical analysis showed that Ca_2SiO_4 was 78-percent Ca_2SiO_4 and 22-percent $CaSiO_3$, -200 + 325 mesh

[g]-150 + 325 mesh

[h]-325 mesh + 10 μm

TABLE V - REACTIONS BETWEEN YTTRIA-STABILIZED ZIRCONIA AND OXIDES AND SULFATES OF VARIOUS ELEMENTS

	Temperature °C (°F)											
	1700 (2160)				1300 (2400)				1400 (2520)			
	Time, hr											
	400		800		200		100		100		200	
Na_2SO_4	ZrO_2 cubic ZrO_2 monoclinic Unknown phase	N[a]	ZrO_2 cubic ZrO_2 monoclinic Unknown phase	N	ZrO_2 cubic ZrO_2 monoclinic Unknown phase	N	ZrO_2 cubic ZrO_2 monoclinic Unknown phase	N	ZrO_2 cubic ZrO_2 monoclinic Unknown phase	N	ZrO_2 cubic ZrO_2 monoclinic Unknown phase	N
Na_2CO_3[b] (Na_2O)	ZrO_2 cubic Na_2ZrO_3	Y[c]	ZrO_2 cubic Na_2ZrO_3	Y	ZrO_2 cubic Na_2ZrO_3	Y	ZrO_2 cubic Na_2ZrO	Y	ZrO_2 cubic Na_2ZrO_3	Y	ZrO_2 cubic Na_2ZrO	Y
K_2SO_4	ZrO_2 cubic ZrO_2 monoclinic Unknown phase	N	ZrO_2 cubic ZrO_2 monoclinic Unknown phase	N	ZrO_2 cubic ZrO_2 monoclinic Unknown phase	N	ZrO_2 cubic ZrO_2 monoclinic Unknown phase	N	ZrO_2 cubic ZrO_2 monoclinic Unknown phase	N	ZrO_2 cubic ZrO_2 monoclinic Unknown phase	N
K_2CO_3[b] (K_2O)	ZrO_2 cubic ZrO_2 monoclinic	Y	ZrO_2 cubic ZrO_2 monoclinic	Y	ZrO_2 cubic ZrO_2 monoclinic	Y	ZrO_2 cubic ZrO_2 monoclinic	Y	ZrO_2 cubic $K_2Zr_4O_9$	Y	ZrO_2 cubic ZrO_2 monoclinic	Y
$BaSO_4$	Not tested		Not tested		Not tested		Not tested		$BaZrO_3$ Unknown phase		$BaZrO$ Unknown phase	
$BaCO_3$[b] (BaO)	$BaZrO_3$	Y	$BaZrO_3$	Y	$BaZrO_3$	Y	$BaZrO$	Y	$BaZrO$	Y	$BaZrO_3$	Y
$CaCO_3$[b] (CaO)	$CaZrO_3$	Y	$CaZrO_3$	Y	$CaZrO_3$	Y	$CaZrO_3$	Y	$CaZrO_3$	Y	$CaZrO$	Y
MgO	ZrO_2 cubic ZrO_2 monoclinic MgO	N	ZrO_2 cubic ZrO_2 monoclinic MgO	N	ZrO_2 cubic ZrO_2 monoclinic MgO	Y	ZrO_2 cubic MgO Trace of monoclinic ZrO_2	Y	ZrO_2 cubic MgO	Y	ZrO_2 cubic MgO	Y
SiO_2	ZrO_2 cubic ZrO_2 monoclinic SiO_2[e] $ZrSiO_4$	Y	ZrO_2 cubic SiO_2 $ZrSiO_4$ Trace of monoclinic ZrO_2	Y	ZrO_2 cubic ZrO_2 monoclinic SiO_2 $ZrSiO_4$	Y	ZrO_2 cubic SiO_2 $ZrSiO_4$	Y	ZrO_2 cubic SiO_2 $ZrSiO_4$	Y	ZrO_2 SiO_2 $ZrSiO_4$	Y
$(NH_4)_2HPO_4$[d] (P_2O_5)	ZrO_2 monoclinic ZrO_2 cubic ZrP_2O_7 $(ZrO)_2P_2O_7$	Y	ZrO monoclinic ZrO_2 cubic ZrP_2O_7 $(ZrO)_2P_2O_7$	Y	ZrO_2 monoclinic ZrO_2 cubic ZrP_2O_7 $(ZrO)_2P_2O_7$	Y	ZrO_2 monoclinic ZrO_2 cubic ZrP_2O_7 $(ZrO)_2P_2O_7$	Y	ZrO_2 monoclinic $(ZrO)_2P_2O_7$	Y	ZrO_2 monoclinic $(ZrO)_2P_2O_7$	Y
V_2O_5	ZrO_2 monoclinic V_2O_5 Unknown phase	Y	ZrO_2 monoclinic V_2O_5 Unknown phase	Y	ZrO_2 monoclinic V_2O_5 Unknown phase	Y	ZrO_2 monoclinic V_2O_5 Unknown phase	Y	ZrO_2 monoclinic V_2O_5 Unknown phase	Y	ZrO_2 monoclinic V_2O_5 Unknown phase	Y
Fe_2O_3	ZrO_2 cubic ZrO_2 monoclinic Fe_2O_3	N	ZrO_2 cubic Fe_2O_3 Trace of monoclinic ZrO_2	Y	ZrO_2 cubic ZrO_2 monoclinic Fe_2O_3	N	ZrO_2 cubic ZrO_2 monoclinic Fe_2O_3	Y	ZrO_2 cubic Fe_2O_3	Y	ZrO_2 cubic Fe_2O_3	Y
Cr_2O_3	ZrO_2 cubic ZrO_2 monoclinic Cr_2O_3	N	ZrO_2 cubic ZrO_2 monoclinic Cr_2O_3	N	ZrO_2 cubic ZrO_2 monoclinic Cr_2O_3	N	ZrO_2 cubic ZrO_2 monoclinic Cr_2O_3	N	ZrO_2 cubic ZrO_2 monoclinic Cr_2O_3	N	ZrO_2 cubic ZrO_2 monoclinic Cr_2O_3	N
Al_2O_3	ZrO_2 cubic ZrO_2 monoclinic Al_2O_3	N	ZrO_2 cubic ZrO_2 monoclinic Al_2O_3	N	ZrO_2 cubic ZrO_2 monoclinic Al_2O_3	N	ZrO_2 cubic ZrO_2 monoclinic Al_2O_3	N	ZrO_2 cubic ZrO_2 monoclinic Al_2O_3	N	ZrO_2 cubic ZrO_2 monoclinic Al_2O_3	N
NiO	ZrO_2 cubic ZrO_2 monoclinic NiO	N	ZrO_2 cubic ZrO_2 monoclinic NiO	N	ZrO_2 cubic ZrO_2 monoclinic NiO	N	ZrO_2 cubic ZrO_2 monoclinic NiO	N	ZrO_2 cubic ZrO_2 monoclinic NiO	N	ZrO_2 cubic ZrO_2 monoclinic NiO	N
$CoCO_3$[b] (CoO)	Not tested		Not tested		Not tested		Not tested		ZrO_2 cubic CoO	Y	ZrO_2 cubic CoO	Y
ZnO	ZrO_2 cubic Unknown phase	Y	ZrO_2 cubic Unknown phase	Y	ZrO_2 cubic Unknown phase	Y	ZrO_2 cubic Unknown phase	Y	ZrO_2 cubic Unknown phase	Y	ZrO_2 cubic Unknown phase	Y

[a] N indicates that no reaction occurred

[b] ZrO_2 was reacted with the oxide indicated in the parentheses Carbonates were the convenient form for handling these oxides

[c] Y indicates a partial or complete reaction

[d] P_2O_5 was introduced in the form of $(NH_4)_2HPO_4$

[e] α-cristobalite

TABLE VI. - CORRELATION COEFFICIENTS FOR CORROSION MODEL

$[\log(\Delta th_i) = a_i + b_i \log(\text{Time}) \pm \sigma.]$

Alloy	Intercept a	Slope b	Standard error of estimate, σ	Thickness change estimated at 200 hr, Δth, μm
IN-100	0.7854	0.9221	0.1945	830
U-700	.1378	1.2844	.2769	1471
IN-792	.5871	.8535	.1256	346
Mar M-509	1.0250	.5383	.1607	186

TABLE VII. - DOPANT COMPOSITIONS

OF COMBUSTION PRODUCTS

Element	Dopant A	Dopant B
	Composition, ppm by weight	
Fe	2.0	2.0
Pb	.05	.05
Ca	.1	.1
Na	5	.5
K	.1	.1
P	---	.5

TABLE VIII. - BURNER RIG

TEST CONDITIONS

Flame temperature		Cooling flow rate,[a] $(\rho V)_c/(\rho V)_h$
^{o}C	^{o}F	
1100	2000	0 4
1220	2200	.9
1300	2400	1 0
1550	2800	2 3
1800	3300	3 8

[a]Where $(\rho V)_c$ = Density × Velocity = Mass flow rate through film-cooling holes. And $(\rho V)_h$ = Density × Velocity = Hot-gas mass flow rate.

TABLE IX - RESULTS OF FILM-COOLING-HOLE PLUGGING TESTS

Flame temperature[a]		Dopant	Cooling flow rate,[b] $(\rho V)_c/(\rho V)_h$	Leading-edge temperature increase	
^{o}C	^{o}F			$^{o}C\pm10$	$^{o}F\pm18$
1300	2400	A	1.0	72	130
1550	2800	A	2 3	11	20
1800	3300	A	3.8	28	50
1100	2000	B	4	39	70
1220	2200	↓	.9	89	160
1300	2400	↓	1 0	111	200
1550	2800	↓	2 3	56	100

[a]Measured with a sonic velocity thermocouple probe.

[b]Where $(\rho V)_c$ = Density × Velocity = Mass flow rate through film-cooling holes And $(\rho V)_h$ = Density × Velocity = Hot-gas mass flow rate.

TABLE X. - SUMMARY OF COMBINED-CYCLE CASES INVESTIGATED

Turbine-inlet temperature		Air-cooled combined cycles				Steam-cooled combined cycles				Water-cooled combined cycles			
		Thermal-barrier coating thickness, cm (in)											
°C	°F	0	[a]0.038 (0.015)	[a]0 076 (0 030)	[b]0.038 (0 015)	0	[a]0.038 (0.015)	[a]0 076 (0 030)	[b]0 038 (0 015)	0	[a]0 038 (0 015)	[a]0 076 (0.030)	[b]0.038 (0 015)
1650	3000									×	×	×	×
1425	2600					×	×	×	×	×	×	×	×
1205	2200	×	×	×	×	×	×	×	×				

[a]Same turbine-inlet temperature as for uncoated system, reduced cooling flow.

[b]Same cooling flow as uncoated system; increased turbine-inlet temperature.

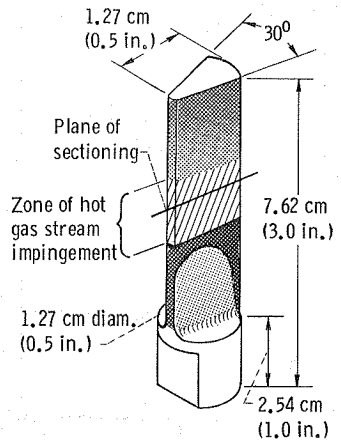

(a) Test bar.

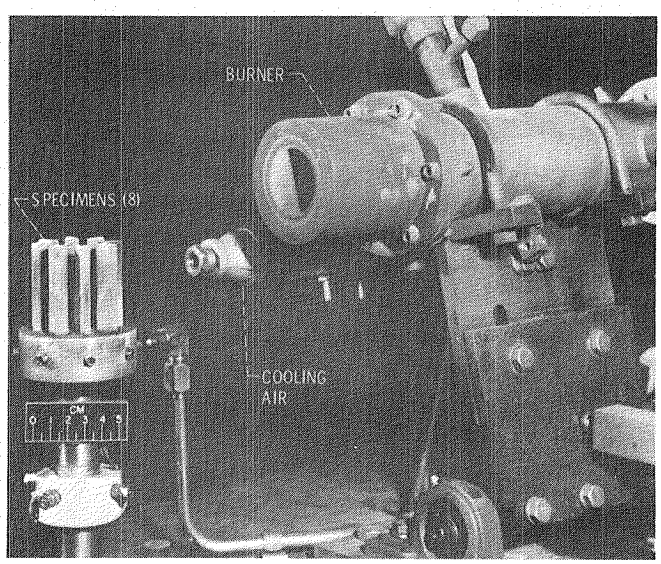

(b) Burner rig.

Figure 1. - Hot-corrosion apparatus and test specimen.

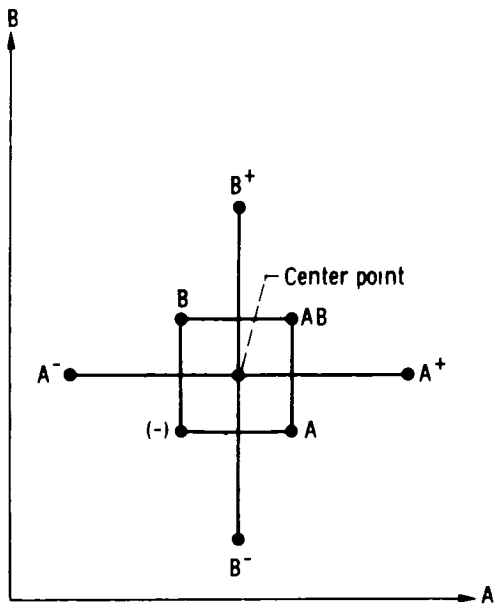

Figure 2 - Two-dimensional star design

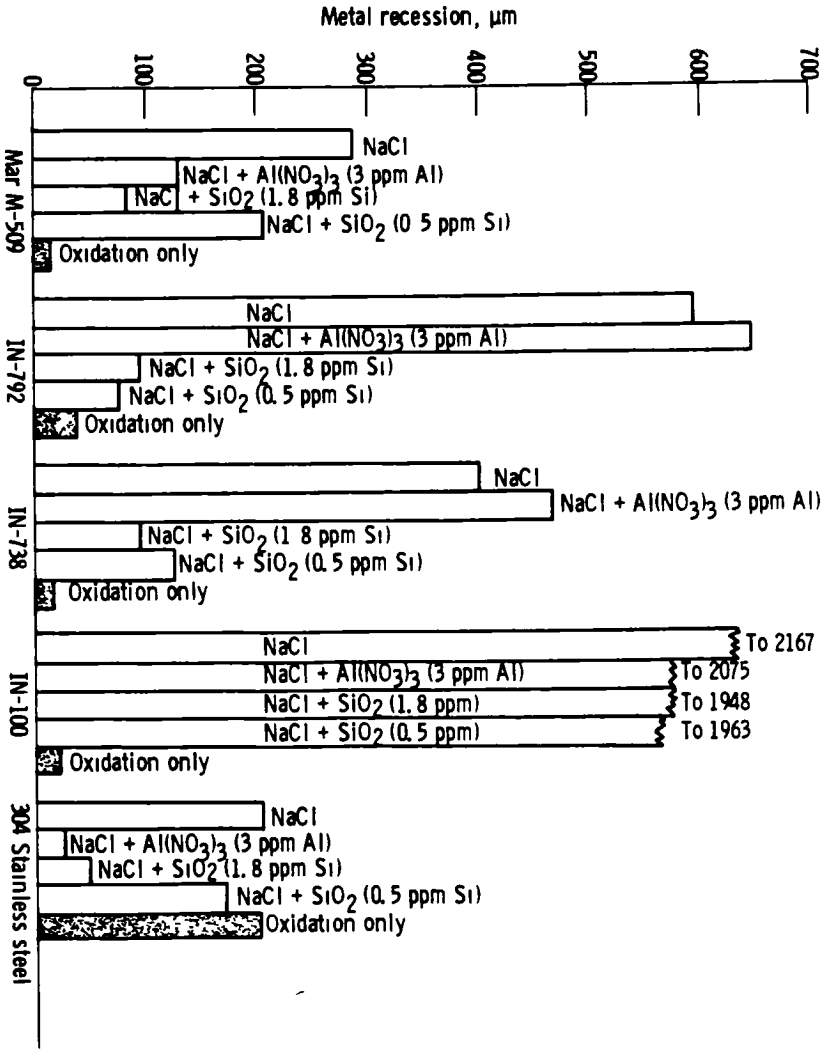

Figure 3. - Effect of aluminum and silicon additions on burner rig hot corrosion after 100 1-hour cycles at 900° C (1652° F) and Mach 0.3

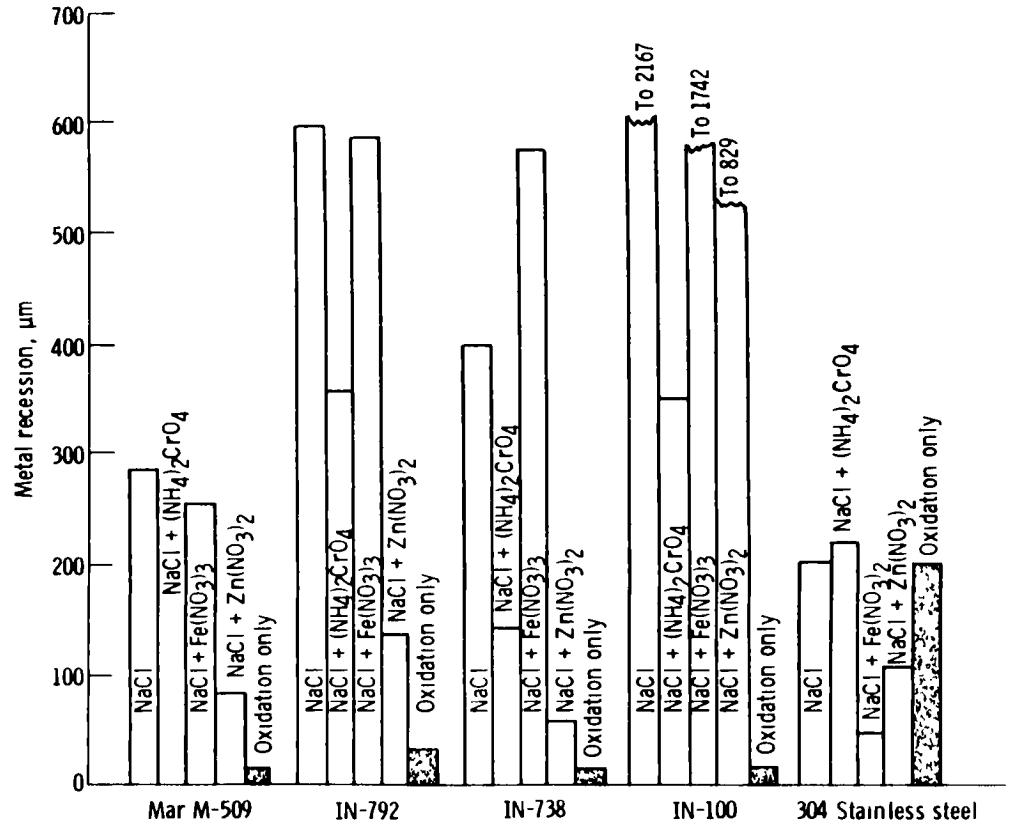

Figure 4 - Effect of chromium, iron, and zinc additions on burner rig hot corrosion after 100 1-hour cycles at 900^0 C (1652^0 F) and Mach 0 3 All additive concentrations are at 3 ppm of each metal

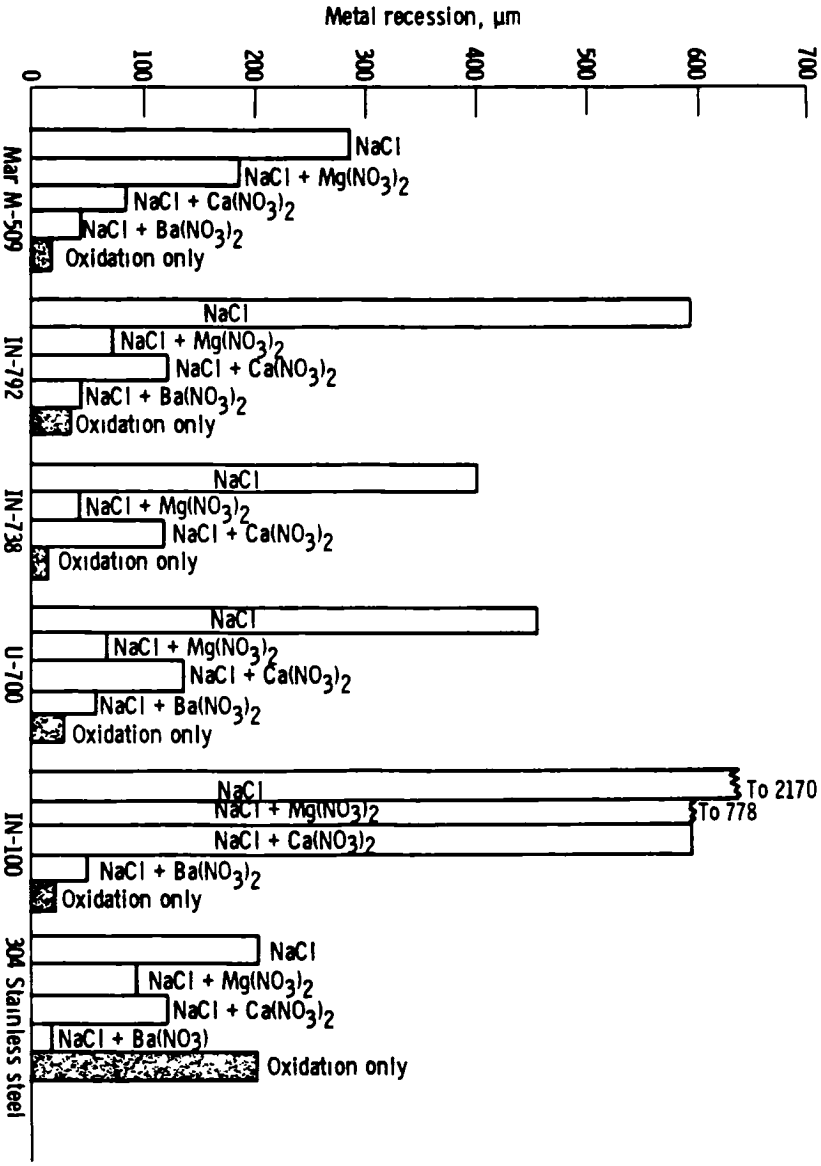

Figure 5. - Effect of alkaline earth additions on burner rig hot corrosion after 100 1-hour cycles at 900° C (1652° F). All additive concentrations are at 3 ppm of each metal

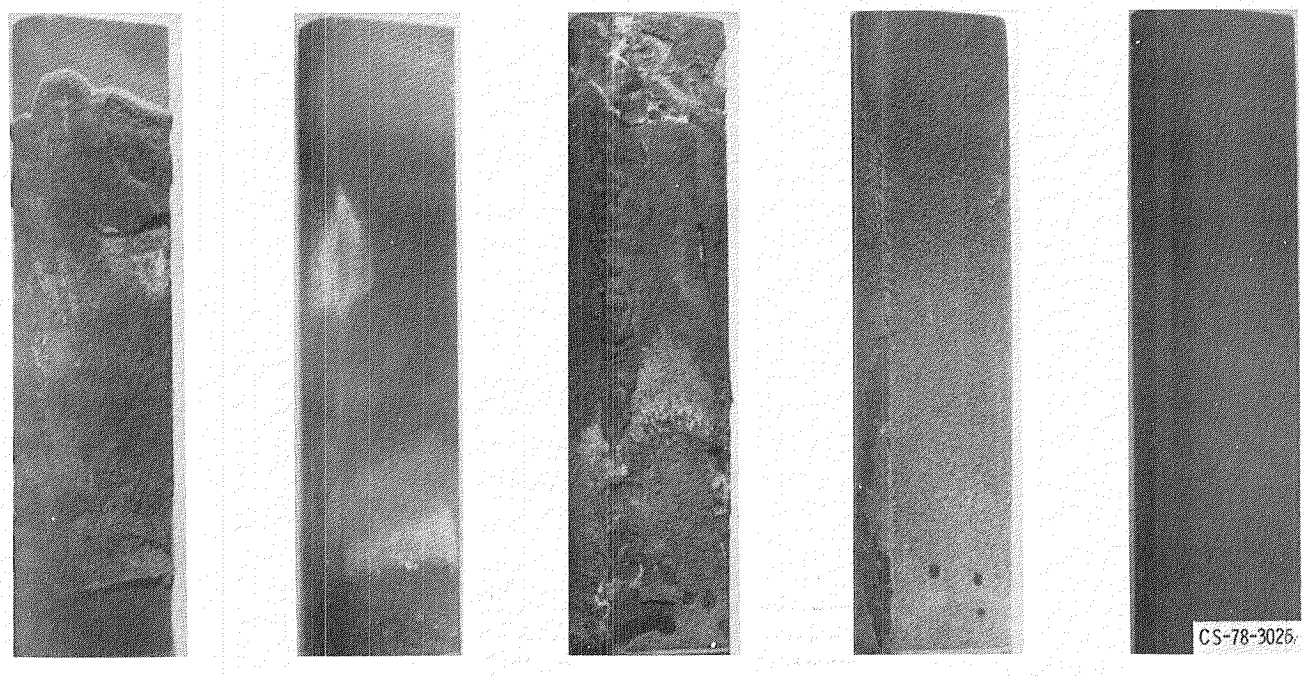

(a) NaCl only. (b) NaCl + $Mg(NO_3)_2$. (c) NaCl + $Ca(NO_3)_2$. (d) NaCl + $Ba(NO_3)_2$. (e) Oxidation only.

Figure 6. - Effect of alkaline earth additions on deposition on and corrosion of IN-792 after 100 1-hour cycles at 900^0 C (1652^0 F) and Mach 0.3. All additive concentrations are at 3 ppm of each metal.

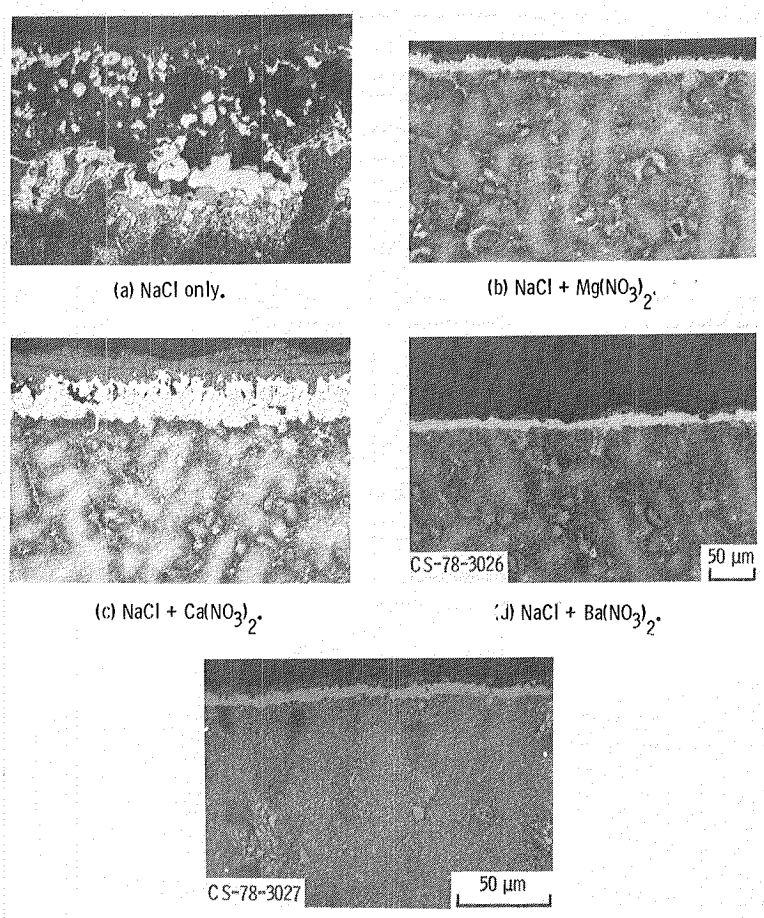

(a) NaCl only. (b) NaCl + $Mg(NO_3)_2$.

(c) NaCl + $Ca(NO_3)_2$. (d) NaCl + $Ba(NO_3)_2$.

(e) Oxidation only.

Figure 7. - Effect of alkline earth additions on microstructure of IN-792 after 100 1-hour cycles at 900^0 C (1652^0 F) and Mach 0.3. All additive concentrations are at 3 ppm of each metal.

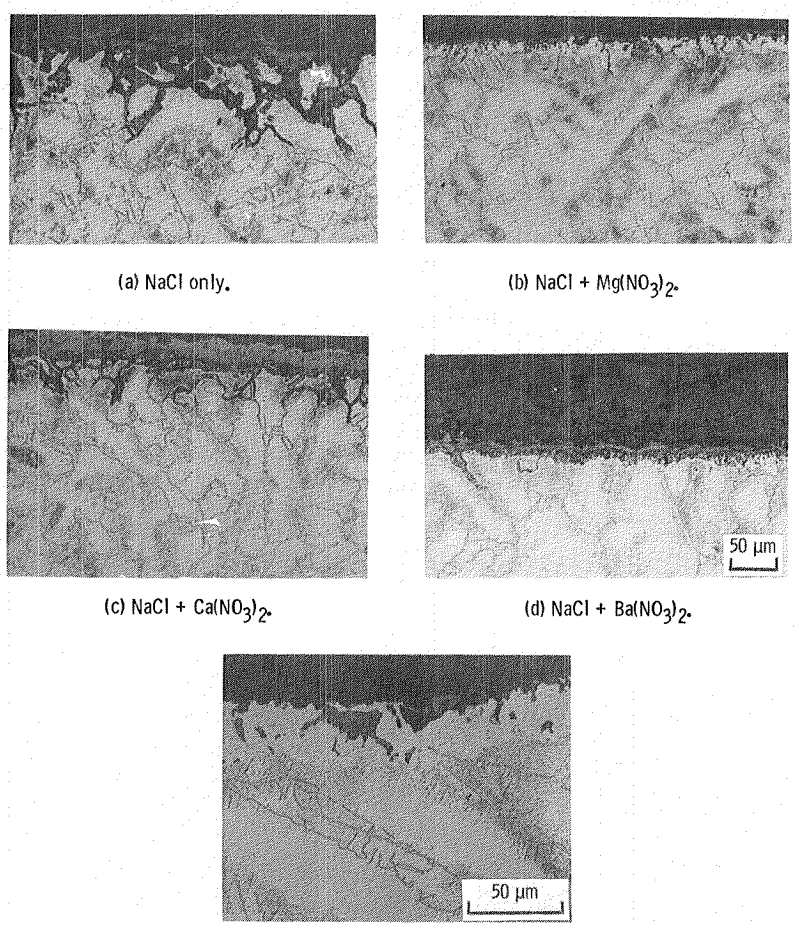

(a) NaCl only.

(b) NaCl + $Mg(NO_3)_2$.

(c) NaCl + $Ca(NO_3)_2$.

(d) NaCl + $Ba(NO_3)_2$.

(e) Oxidation only.

Figure 8. - Effect of alkaline earth addition on microstructure of Mar-M-509 after 100 1-hour cycles at 900^0 C (1652^0 F) and Mach 0.3. All additive concentrations are at 3 ppm of each metal.

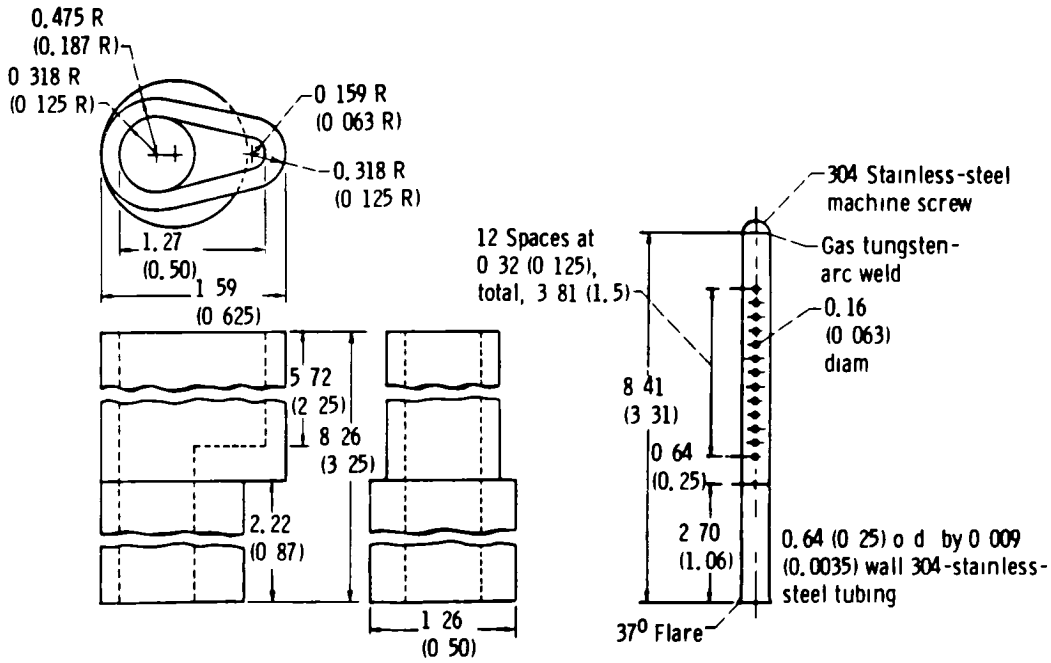

(a) Cast-superalloy hollow erosion bar

(b) Cooling insert

Figure 9 - Hollow erosion bar and air-cooling insert (Dimensions are in cm (in))

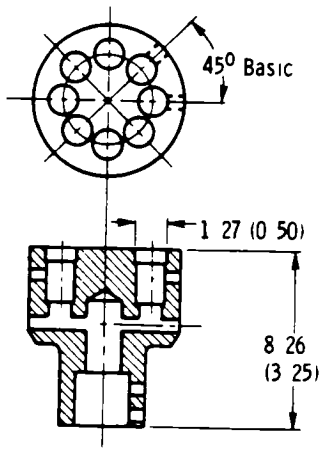

Figure 10 - Multiple-specimen test fixture (Dimensions are in cm (in))

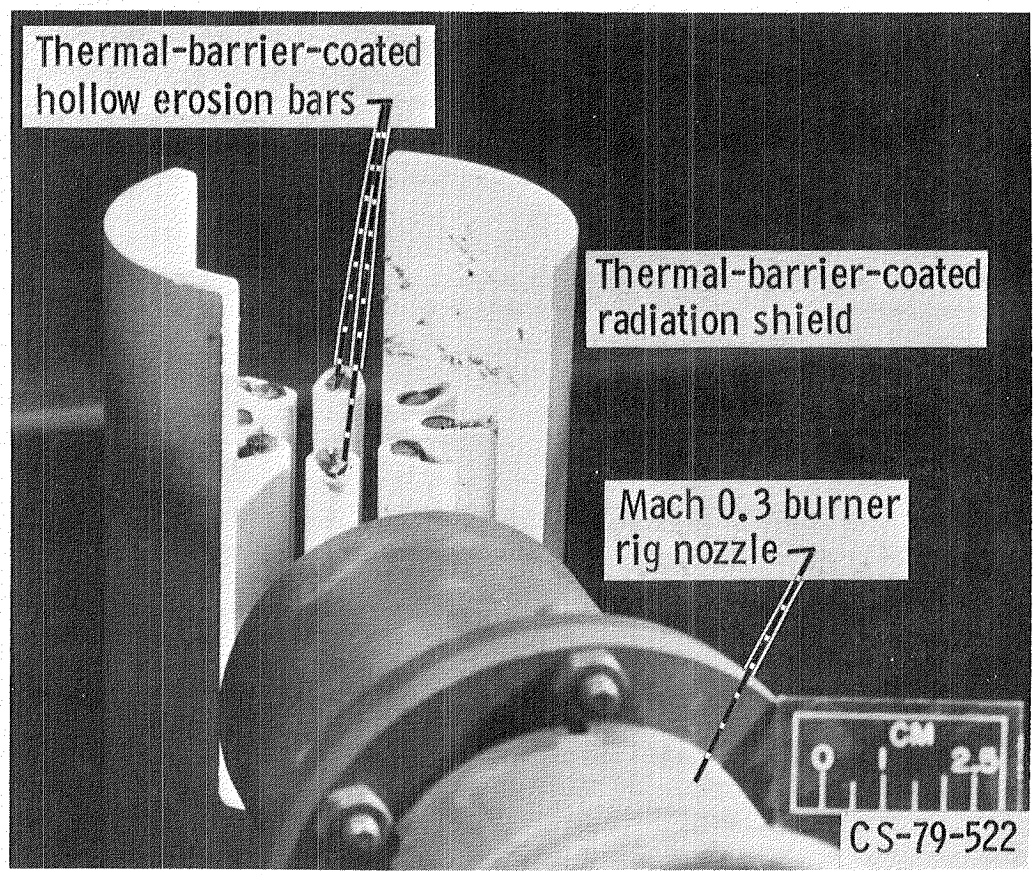

Figure 11. - Mach 0.3 burner rig and thermal-barrier-coated IN-792 hollow erosion bars.

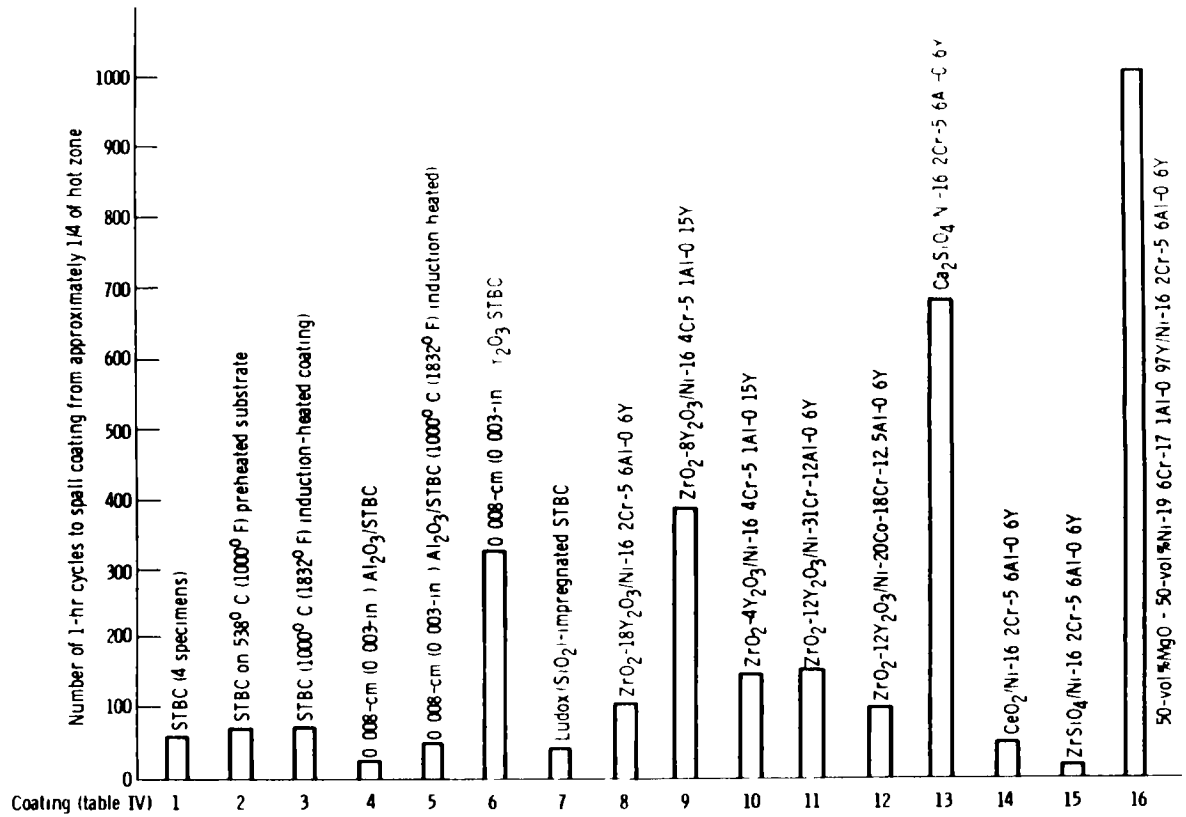

Figure 12 - Multiple-specimen Mach 0 3 burner rig test of thermal-barrier coating systems on IN-792 cooled hollow erosion bars Operating conditions fuel impurity equivalent of 5 ppm Na + 2 ppm V, flame temperature 1370° C (2500° F), metal-substrate temperature, 843° C (1550° F) ceramic surface temperature 982° C (1800° F) (STBC denotes standard thermal-barrier coating, ZrO_2-12Y_2O_3/Ni-16 2Cr-5 6Al- 6Y)

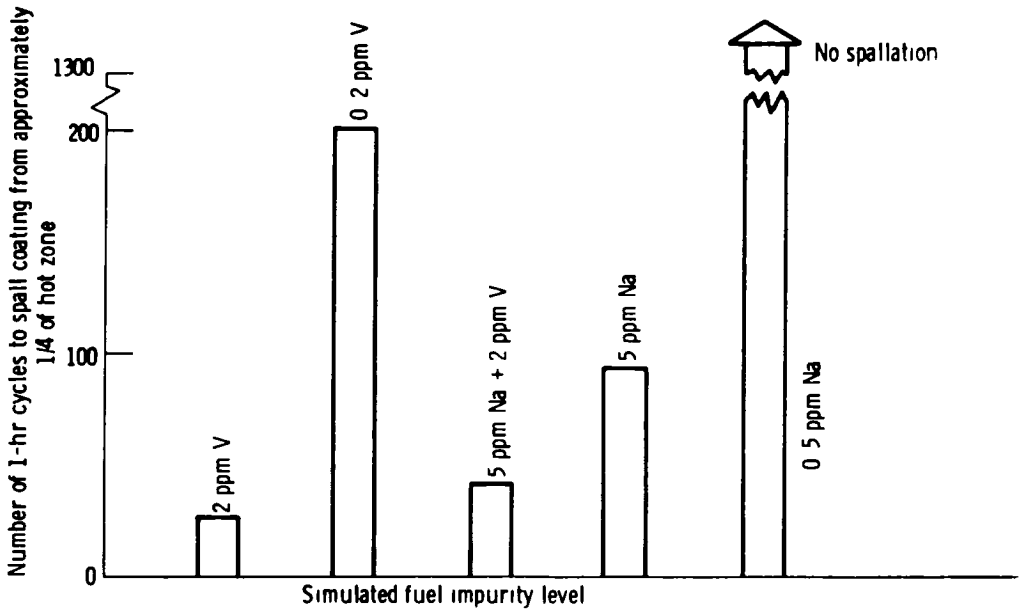

Figure 13 - Single-specimen Mach 0 3 burner rig tests of ZrO_2-12Y_2O_3/NiCrAlY thermal-barrier coating system to fuel impurities Operating conditions flame temperature, 1370° C (2500° F), metal-substrate temperature, 843° C (1550° F), ceramic-surface temperature, 982° C (1800° F)

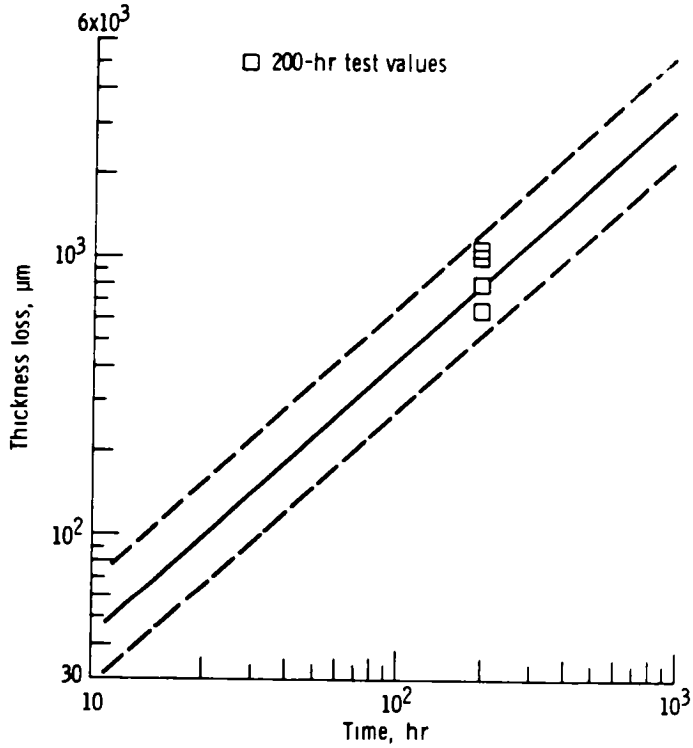

Figure 14 - Hot-corrosion-thickness-loss prediction model for IN-100

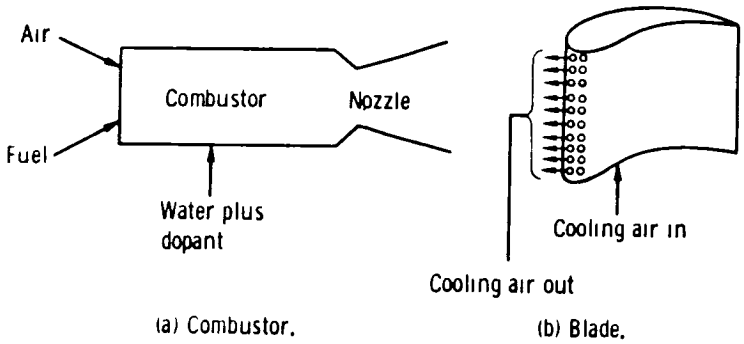

(a) Combustor. (b) Blade.

Figure 15. - Schematic diagram of burner rig.

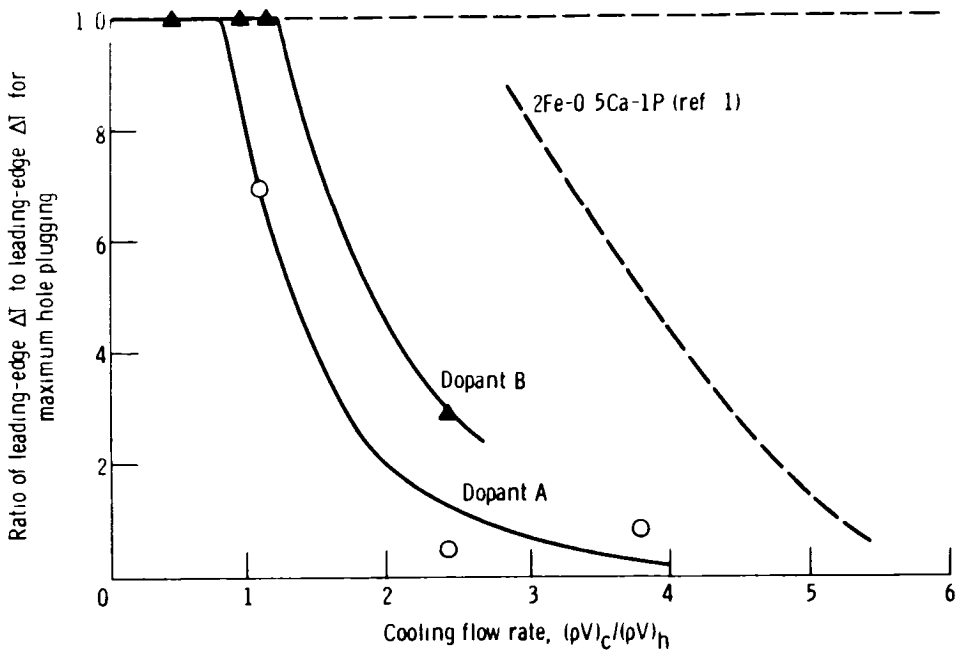

Figure 16 - Effect of cooling flow rate on plugging of showerhead film-cooling holes

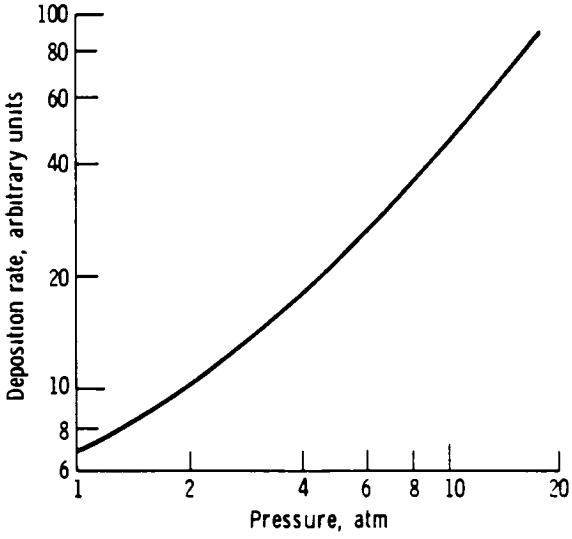

Figure 17 - Calculated effect of pressure on deposition rate of $NaSO_4$ Temperature, 800° C (1472° F)

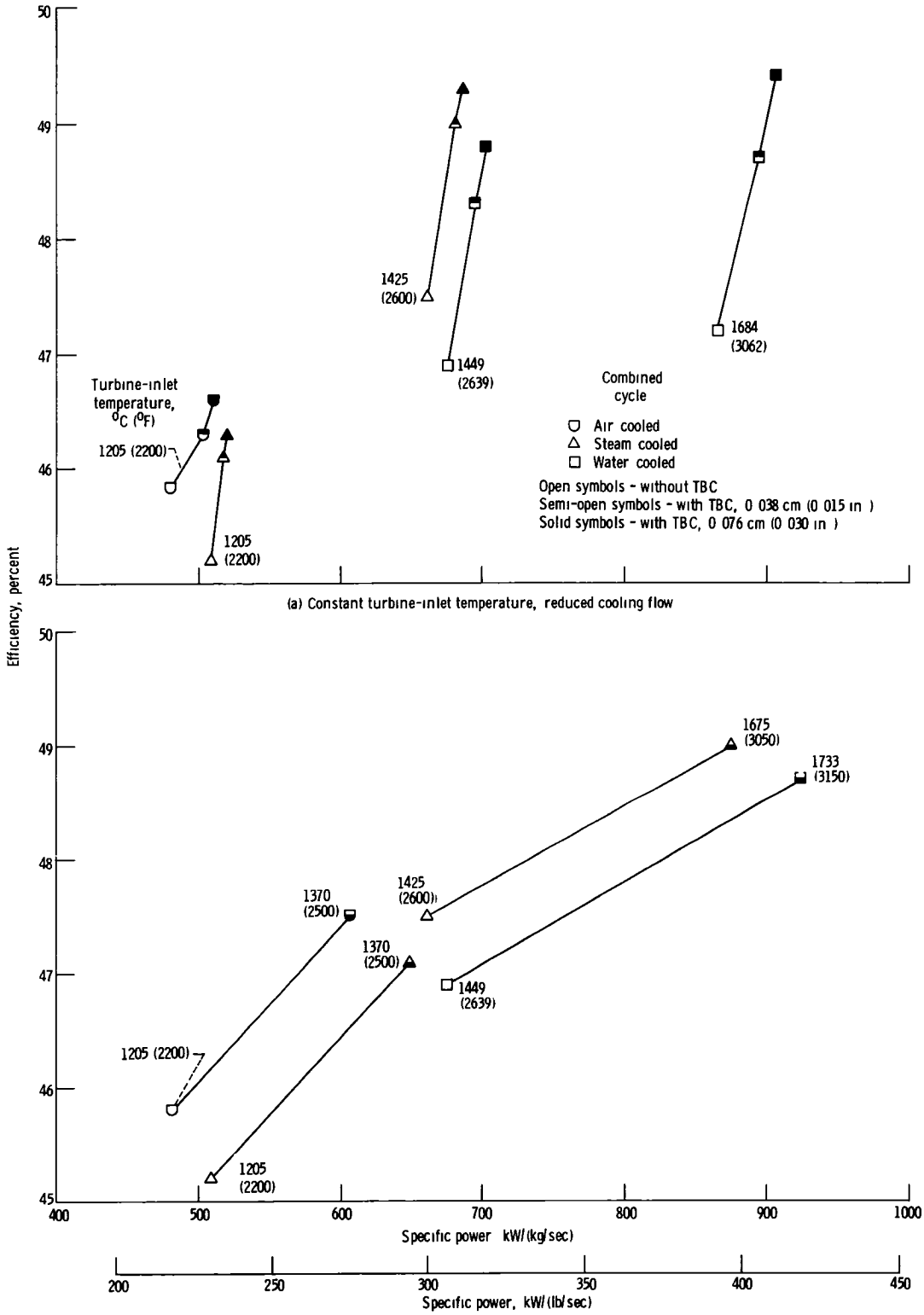

Figure 18 - Combined-cycle performance gains with thermal-barrier coatings

End of Document